water

MDPI

Article

Heterogeneous Catalytic Ozonation of Aniline-Contaminated Waters: A Three-Phase Modelling Approach Using TiO_2/GAC

Cristian Ferreiro [1,*], Natalia Villota [2], José Ignacio Lombraña [1] and María J. Rivero [3]

[1] Department of Chemical Engineering, Faculty of Science and Technology, University of the Basque Country UPV/EHU, Barrio Sarriena s/n, 48940 Leioa, Spain; ji.lombrana@ehu.eus
[2] Department of Chemical and Environmental Engineering, Faculty of Engineering Vitoria-Gasteiz, University of the Basque Country UPV/EHU, Nieves Cano 12, 01006 Vitoria-Gasteiz, Spain; natalia.villota@ehu.eus
[3] Department of Chemical and Biomolecular Engineering, University of Cantabria, 39005 Santander, Spain; riveromj@unican.es
* Correspondence: cristian.ferreiro@ehu.eus; Tel.: +34-946-012-512

Received: 30 October 2020; Accepted: 3 December 2020; Published: 8 December 2020

Abstract: This work aims to study the sustainable catalytic ozonation of aniline promoted by granular active carbon (GAC) doped with TiO_2. Aniline was selected as a model compound for the accelerator manufacturing industries used in the manufacture of rubber due to its environmental impact, low biodegradability, and harmful genotoxic effects on human health. Based on the evolution of total organic carbon (TOC), aniline concentration measured using high performance liquid chromatography (HPLC), pH and ozone concentration in liquid and gas phase, and catalyst loading, a three-phase reaction system has been modelled. The proposed three-phase model related the ozone transfer parameters and the pseudo-first order kinetic constants through three coefficients that involve the adsorption process, oxidation in the liquid, and the solid catalyst. The interpretation of the kinetic constants of the process allowed the predominance of the mechanism of Langmuir–Hinshelwood or modified Eley–Rideal to be elucidated. Seven intermediate aromatic reaction products, representative of the direct action of ozone and the radical pathway, were identified and quantified, as well as precursors of the appearance of turbidity, with which two possible routes of degradation of aniline being proposed.

Keywords: aniline; catalytic ozonation; degradation routes; industrial wastewater; three-phase system; TiO_2/GAC

1. Introduction

At present, as part of corporate social responsibility, manufacturing industries must compromise in the short-term in order to carry out environmental protection actions. A report from the United Nations has indicated that, in 2015, more than 80% of the wastewaters of worldwide human activities were being discharged into rivers and sea without the removal of polluting substances [1]. Despite the fact that manufacturing companies have been opting for environmentally sustainable processes, the Sustainable Development Goals (SDGs) are unfortunately far from being met in 2030 [2]. In this work, the removal of aniline, as a model pollutant of environmental concern, is studied. Aniline (ANI) is mainly used in the synthesis of methylene diphenyl isocyanate to produce polyurethane foams, antioxidants, activators, and accelerators in the rubber industry, as well as in the synthesis of indigo and other dyes [3]. It is also employed as a raw material in the manufacturing of different types of fungicides in the agricultural and pharmaceutical industries [4,5].

The uncontrolled discharge of industrial effluents containing aniline is harmful to both humans and the environment. In humans, it has been well-documented to induce carcinogenic, teratogenic, and mutagenic effects [6]. Acute exposure to high amounts of aniline (>1 g) for a 75 kg person could lead to coma or even death [7]. In addition, uncontrolled discharges containing aniline could disturb the aquatic environment, causing mortality in aquatic animals and plants [4]. High concentrations of aniline in rivers and groundwater could affect crop safety and, consequently, human health. Studies of aniline genotoxicity in plants have also been carried out, which concluded that it significantly inhibits the growth of wheat crops irrigated with water contaminated with aniline at a concentration of 25 mg L^{-1} [8]. Therefore, aniline has garnered great attention and has been classified as a persistent organic pollutant by the U.S. Environmental Protection Agency [9]. Conventional treatment systems based on biological processes are not suitable for the treatment of wastewater contaminated with aniline, due to micro-organism deactivation. Hence, new treatment technologies are needed, in order to transform aniline into biodegradable substances of lower toxicity before conducting biological treatment [6,8].

The removal of aniline from contaminated water has been a topic of concern for several research groups, as shown in Table 1. According to Table 1, in most studies a high degree of mineralization and degradation of the aniline was not achieved. Additionally, most of the treatment technologies for aniline removal require complex equipment, which are costly and have limited potential for full-scale implementation in wastewater treatment plants. Among such technologies, heterogeneous catalytic ozonation based on the use of TiO_2/granular active carbons (GAC) has emerged as a sustainable and cost-effective (0.64 Euro per kg of total organic carbon (TOC) eliminated) treatment alternative for the removal of aniline from contaminated waters [4]. An increase in the number of scientific reports has indicated the successful development of new activated carbon types modified through the incorporation of metal oxides with enhanced catalytic activity, thus endorsing the application of this catalytic technology at industrial scale [10,11]. The improvement in the removal yields can be attributed to the ozonation mechanisms that take place on catalytic surfaces. These mechanisms have not yet been fully defined [12]. One mechanism postulated is that the catalyst acts as an adsorbent where organic contaminants are first adsorbed on the catalyst surface and then removed [13]. The other mechanism proposed suggests that the titanium oxides favours ozone mass transport and initiates its decomposition. This mechanism assumes that the hydroxyl groups on the catalytic surface play an important role in the generation of the radical species [14].

In order to fulfil the industrial implementation requirements of this new catalytic technology, the prediction of operating behaviour under different working conditions becomes a critical point, which is yet to be solved. Delmas et al. [15] modelled a sequential process based on adsorption onto activated carbon followed by a wet catalytic oxidation with ozone. However, only a few studies have focused on the prediction and estimation of the effects of the main operational variables (e.g., pH, ozone dose, and catalyst load), as well as the contribution of chemical surface properties of TiO_2/GAC composite during the heterogeneous catalytic ozonation of wastewater containing aniline [16–19]. The study presented here addresses such challenges. In particular, we aim to develop a three-phase modelling approach that includes mass transfer parameters and rate constants from both surface and liquid bulk reactions which allow for the establishment of operating conditions that: (i) enhance radical generation due to ozone decomposition promoted by the TiO_2/GAC composite and (ii) avoid both catalyst deactivation and deterioration of the physical–chemical properties of the GAC.

Table 1. Previous studies regarding the treatment of industrial wastewater containing aniline.

Treatment	Catalyst	Operating Conditions	Comments	References
Ozone	—	(Time) = 120 min; C_0 = 103.81 mg L^{-1}; pH = 7.0; T = 20 °C; F_G = 2.5 g h^{-1}; $C_{O_3,G}$ = 22.0 mg L^{-1}; (%) = 93.56%; (% COD) = 31.03%	Studied the effect of operational variables on the biodegradability of aniline oxidation by-products, highlighting among them diacid butane, oxalic acid, and formic acid.	[6]
US/O_3	—	(Time) = 30 min; C_0 = 100 mg L^{-1}; pH_0 = 7.0; T = 25 °C; F_G = 12 mg min^{-1}; $US_{density}$ = 0.1 W mL^{-1}; (%) = 99%; (% TOC) = 51%	The synergistic effect improved the degradation and mineralization of aniline by 64% and 110% respectively in terms of total organic carbon (TOC) compared to simple ozonation.	[20]
O_3/GAC	GAC (Norit® 1240 Plus granular activated carbon (Cabot Norit Americas, Inc., Marshall, TX, USA))	(Time) = 30 min; C_0 = 102.44 mg L^{-1}; pH = 7.0; T = 25 °C; F_G = 150 cm^3 min^{-1}; $C_{O_3,G}$ = 50.0 mg L^{-1}; (%) = 100%; (% TOC) = 56%; M_{CAT} = 500 mg L^{-1}	Studied the catalytic effect of GAC on the ozonisation process. Basic GACs had a higher capacity for decomposition of O_3 and organics adsorption.	[21]
O_3/TiO_2-GAC	TiO_2/GAC (Nanocyl® 3100 activated carbon doped with TiO_2 by hydration–dehydration method (Nanocyl SA, Sambreville, Belgium))	(Time) = 60 min; C_0 = 93.13 mg L^{-1}; pH = 5.6; T = 25 °C; F_G = 150 cm^3 min^{-1}; $C_{O_3,G}$ = 50.0 mg L^{-1}; (%) = 100%; (% TOC) = 57%; M_{CAT} = 500 mg L^{-1}	A higher mineralization was observed when doping the GAC with TiO_2 oxides. The absence of NH_4^+ promoted a different oxidation mechanism compared to pristine GAC.	[22]
	TiO_2/GAC (Norit® 1240 Plus granular activated carbon doped with TiO_2 by precipitation method (Cabot Norit Americas, Inc., Marshall, TX, USA))	(Time) = 45 min; C_0 = 20.0 mg L^{-1}; pH = 7.0; T = 18 °C; F_G = 2.5 g h^{-1}; $C_{O_3,G}$ = 5.4 mg L^{-1}; (%) = 100%; (% TOC) = 80.24%; M_{CAT} = 3.33 g L^{-1}	Through a novel method of synthesis by precipitation, a high yield was obtained in terms of degradation and mineralization.	[4]
TiO_2/UV	Hybrid Suspended-Supported TiO_2	(Time) = 4.73 h; C_0 = 22 mg L^{-1}; M_{CAT} = 60 mg L^{-1}; (*Supp. Cat.*) = 2.3 mg cm^{-2}; pH = 12.0; T = 25 °C; (%) = 99%	Under favourable operating conditions, using a hybrid system with suspended TiO_2 catalyst, a 23% improvement in the elimination of aniline was observed compared to supported catalyst.	[5]

2. Materials and Methods

2.1. Materials

The granular activated carbon Norit® GAC 1240 Plus was used as a parent material (provided by the Cabot Corporation, Marshall, TX, USA) with an average particle size of 1.4 mm. The GAC was chemically modified and TiO_2 was introduced using a wet precipitation method already described elsewhere [4]; this combination is denoted as TiO_2/GAC. Both activated carbon samples have been previously characterized [4]; Table 2 summarizes their key textural and chemical surface properties. Textural characteristics, such as specific surface area (S_{BET}), micropore (V_{micro}) and mesopore (V_{meso}) volumes, and average pore diameter (D_p), were obtained by observing N_2 adsorption–desorption isotherms at 77 K [4]. The pH of the point of zero charge (pH_{pzc}) was determined using an acidimetric–alkalimetric titration method [5]. The bulk chemical composition of GAC samples was measured using X-ray fluorescence (XRF), as described previously [4]. The XRF results indicate that the parent GAC is mainly composed of SiO_2 (5.61%) and Al_2O_3 (0.45%), followed by Fe_2O_3 (0.28%), CaO (0.12%), S (0.08%), MgO (0.05%), Na_2O (0.04%), TiO_2 (0.03%), and MnO (0.01%). After the applied modification treatment to the parent GAC, the TiO_2/GAC sample was principally comprised of TiO_2 (9.33%) and SiO_2 (7.01%), followed by Al_2O_3 (1.00%), Fe_2O_3 (0.25%), CaO (0.11%), S (0.19%), Cl (2.53%), MgO (0.22%), Na_2O (0.04%), and MnO (0.01%), as determined using XRF.

Table 2. Textural and chemical surface properties of the parent and modified GAC samples [4].

Samples	S_{BET} ($m^2\ g^{-1}$)	V_{micro} ($cm^3\ g^{-1}$)	V_{meso} ($cm^3\ g^{-1}$)	D_p (Å)	pH_{pzc}
Norit® GAC 1240 Plus	967.0	0.32	0.16	36.8	7.4
TiO_2/GAC	985.0	0.29	0.16	33.9	6.4

2.2. Analytical Methods

Aniline concentration was measured using HPLC with a Waters Alliance 2695 liquid chromatograph (Waters, Milford, CT, USA) equipped with an Agilent ZORBAX® Rapid Resolution High Definition (RRHD) Eclipse PAH threaded column (150 mm × 4.6 mm, 5 µm) (Agilent Technologies, Palo Alto, CA, USA) with a guard column and kept at 20 °C. A volume of 20.0 µL of sample was injected. A water:methanol (80:20 *v*/*v*) solution was used as a mobile phase with a flow-rate of 1.0 mL min^{-1}. Aniline was detected using a Waters 996 UV-DAD detector (Waters, Milford, CT, USA) at 230 nm.

Aniline oxidation by-products were identified using liquid chromatography coupled to mass spectrometry (MS) in an Agilent 6530 Q-TOF LC/MS (Agilent Technologies, Palo Alto, CA, USA). The separation was carried out using a Kinetex EVO® C18 column (100 mm × 3 mm, 2.6 µm) (Phenomenex, Torrance, CA, USA) kept at 35 °C. A 5.0 µL volume of sample was injected using a flow of 0.3 mL min^{-1}. A mobile phase A consisting of water and a mobile phase B of acetonitrile both containing 0.1% (*v*/*v*) HCOOH were used. The elution started with 20% of B and was maintained for 2 min. Then, the concentration of B was increased until it reached 100% at 22 min. The concentration was kept stable for 4 min and a new separation started after 2 min. MS detection was carried out in the positive voltages, following the optimization of electrospray ionization (ESI) parameters. A nitrogen flow of 10 L min^{-1}, a capillary voltage of 3500 V, a nebulizer pressure of 20 psi, and a source temperature of 350 °C were applied. Calibration curves were formed using aqueous solutions of external standards of known composition.

The degree of mineralization was quantified following the total organic carbon (TOC) concentration using a Shimadzu TOC-VCSH analyzer (Izasa Scientific, Alcobendas, Spain). Turbidity was determined using a turbidimeter EUTECH TN-100 from Thermo Scientific (Thermo Scientific, Singapore).

Chemical surface functionalities of pristine and spent GAC samples were identified using Fourier-transform infrared spectroscopy (FTIR). GAC samples were ground in an agate mortar and the

resulting powders were mixed with anhydrous KBr to yield a mix with 0.5 % *w/w* of GAC. A pressed disc of the mixed sample was placed in a disc holder in a JASCO 4200 spectrometer (JASCO Corporation, Tokyo, Japan) equipped with a DLaTGS detector. Spectra were acquired in transmittance mode in the range 4000–400 cm^{-1} with an average of 64 scans and at a resolution of 4 cm^{-1}, using Spectra Manager software V 2.14.02 (JASCO Corporation, Tokyo, Japan). A pressed disc of pure KBr was used as a background for each measurement.

2.3. Experimental Set Up of The Catalytic Ozonation System

Catalytic ozonation experiments were conducted in a 2 L semi-batch jacketed slurry reactor equipped with a magnetic stirrer and several ozone gas diffusers (see Figure 1). The experiments were carried out using a fixed volumetric flow of ozone (Q_G = 4 L min^{-1}) at different pH conditions (3.0, 5.0, 7.0, and 9.0), with varying ozone doses in the gas phase (3.7, 5.4, 11.3, and 20.1 mg L^{-1}) and catalyst load (1.6, 3.3, 6.6, and 13.3 g L^{-1}).

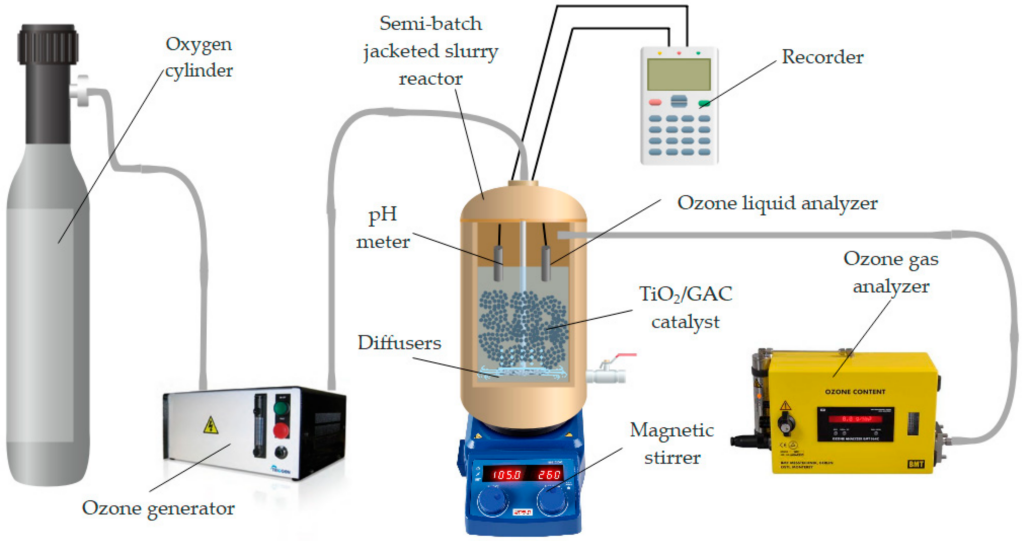

Figure 1. Experimental set-up used to carry out catalytic ozonation tests.

In this study, a concentration of 20.0 mg L^{-1} of aniline—a typical value found in industrial effluent discharges—was used [10,11]. In a typical experiment, the reactor was charged with a 1.5 L solution of aniline at a selected pH value and catalyst load. All experiments were carried out at an authorised discharged temperature of 18 °C and 60 rpm. Ozone was generated in situ from ultra-pure oxygen using a TRIOGEN LAB2B ozone generator (BIO UV, Lunel, France). Ozone concentration in the gas phase was monitored using a BMT 964C ozone analyzer (BMT MESSTECHNIK GMBH, Stahnsdorf, Germany). Dissolved ozone concentration and temperature were measured using a Rosemount 499AOZ-54 dissolved sensor (Emerson, Alcobendas, Spain). The pH value was registered with a Rosemount Analytical model 399 sensor integrated into a Rosemount Analytical Solu Comp II recorder (Emerson, Alcobendas, Spain).

Mass-transfer characterization of the reactor was performed using deionized water in the presence of TiO_2/GAC catalyst, following a procedure previously described by Rodríguez et al. [23]. Operating conditions were kept similar to those used in the presence of aniline. Ozone concentrations in the gas and liquid phases were monitored as described above. All experiments were conducted in duplicate with a maximum standard deviation in concentration measurements not exceeding 0.1 mg L^{-1}.

3. Results and Discussion

3.1. Mathematical Modelling Approach Using TiO_2/GAC Catalysts

3.1.1. Ozone Kinetic Mass Transfer Modelling

In catalytic ozonation processes, mass transfer is considered to be one of the most important stages in the elimination of organic compounds from industrial wastewater. The transfer of ozone from the gas phase to the aqueous phase is often a controlling step in the process [24]. Therefore, effective ozonation is necessary to improve the oxidation of those compounds that are not highly biodegradable and refractory. Thus, the effect of operational variables involved in the transfer of ozone to the liquid (N_{O_3}, mg L^{-1} min^{-1}) through the overall mass transfer coefficient of ozone gas to water ($K_G a$) or $K_L a$ is expressed as follows:

$$N_{O_3} = K_G a \times \left(P_{O_3} - P^*_{O_3}\right) = K_L a \times \left(C^*_{O_3,L} - C_{O_3,L}\right) = \frac{Q_G}{V_{reac}} \times \left(C_{O_3,in} - C_{O_3,out}\right) \quad (1)$$

For calculation of the mass transfer coefficient ($K_L a$) through the second equality, the contactor was considered to be a perfectly mixed semi-continuous reactor. Equation (1) describes the transfer of ozone from the gas to the aqueous phase during the isothermal catalytic ozonation process, where $K_L a$ is the volumetric ozone mass transfer coefficient (min^{-1}), $C^*_{O_3,L}$ is the concentration of dissolved ozone in the liquid phase at saturation conditions (mg L^{-1}), V_{reac} is the volume of reaction solution (L), Q_G is the flow rate of ozone gas at the inlet (L min^{-1}), and $C_{O_3,in}$ and $C_{O_3,out}$ are the concentrations of ozone in the gas phase at the inlet and outlet, respectively (mg L^{-1}).

According to Rodriguez et al. and Schulz and Prendiville [23,25], in this study, the mass transfer resistance in the gas phase was considered negligible compared to that of the liquid. Consequently, the mass transfer coefficient $K_L a$ can be influenced by the volumetric gas flow, the pH of the solution, the bubble size, and mixing regime, among others. A correctly designed ozone contactor should have a good ozone transfer, avoiding mass transfer control in order to achieve a high mineralization

For determination of the $K_L a$ coefficient, the ozone concentration in the liquid at equilibrium was determined through Henry's law, according to Equation (2):

$$C^*_{O_3,L} = P_{O_3}/\mathrm{He} \quad (2)$$

where Henry's solubility constant (atm mole fraction^{-1}) was estimated through Roth and Sullivan's correlation [26]:

$$\mathrm{He} = 3.84 \times 10^7 \times C^{0.035}_{OH^-} \times \exp\left(-\frac{2428}{T}\right), \quad (3)$$

where C_{OH^-} is the concentration of hydroxyl ions (mol L^{-1}) and T is the system temperature (K). Through the execution of a calculation program with Scilab® software version 6.1.0 (Scilab Enterprises, Rungis, France), the $K_L a$ values (with a determination coefficient of $R^2 \cong 0.99$) were determined for different pH values and ozone doses at the reactor input. Figure 2 shows the estimated values of the mass transfer constant as a function of pH maintaining a constant ozone dose (11.3 mg L^{-1}) and as a function of ozone dose maintaining a constant neutral pH of 7.0 for an ozonation system with TiO_2/GAC catalyst in the absence of a pollutant.

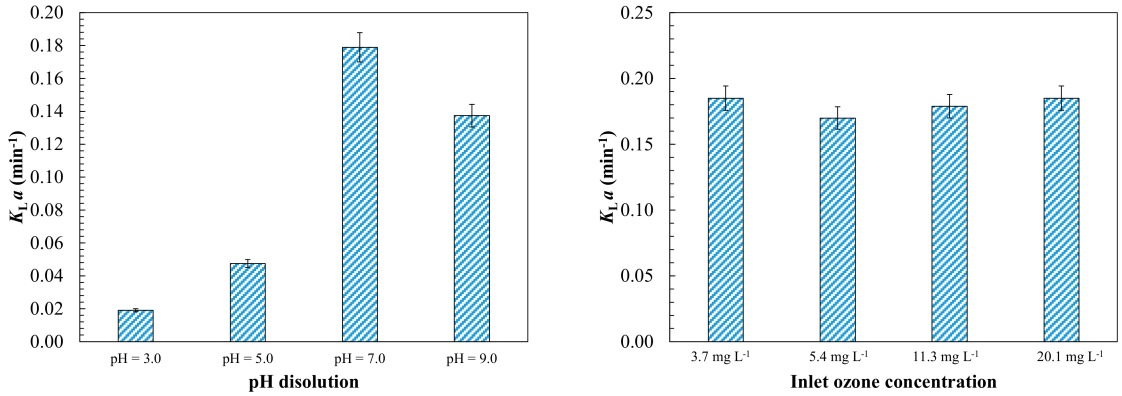

Figure 2. Comparison of volumetric mass transfer coefficient: (**a**) influence of pH on $K_L a$ [1] and (**b**) effect of inlet ozone concentration on $K_L a$ [2]. Experimental conditions: Q_G = 4 L min^{-1}; M_{CAT} = 3.3 g L^{-1}; T = 18.0 °C; P = 1 atm; V_{reac} = 1.5 L; (*Agitation*) = 60 rpm. [1] $C_{O_3,in}$ = 11.3 mg L^{-1}; [2] pH = 7.0.

According to Figure 2a, an increase in the mass transfer coefficient was obtained by increasing the pH of the solution. This is due to the fact that the solubility of ozone in water decreases in acid (pH ≅ 2–3) and alkaline (pH ≅ 8–12) solutions [27]. Under acidic conditions, the decrease in solubility is due to the formation of protonated ozone. This is because the protonation of ozone by the hydronium ion (H_3O^+) is thermodynamically unfavourable and the reverse reaction leads to a lower activation energy, which consequently leads to a decrease in solubility [28,29]. On the other hand, under alkaline conditions (pH > 8), the decrease in ozone solubility in water is associated with the self-decomposition of ozone due to the catalytic action of hydroxyl radicals.

The mass transfer coefficients obtained were of the same order of magnitude as those found by other authors [23,30,31], emphasizing the significant increase at pH = 7.0, where Rodríguez et al. [23] obtained a coefficient of 0.073 min^{-1}.

In Figure 2b, the mass transfer coefficients obtained at different ozone doses compared while maintaining a pH of 7.0 are shown. It was found that the dose of ozone had no significant effect on the obtained $K_L a$ values. As can be seen, the mass transfer coefficient was independent of the input gas concentration, which was 0.182 min^{-1}. The same $K_L a$ obtained at different inlet ozone concentrations is due to the fact that an increase in the ozone concentration in the gas simultaneously produces an increase in the amount adsorbed and in the driving gradient ($C^*_{O_3,L} - C_{O_3,L}$). This confirms that ozone transfer is controlled by the liquid phase, as reported by Berry et al. [32] in a study using membranes and different doses of ozone injected into the reaction system.

According to the results obtained, it is suggested that these transfer coefficients depend mainly on other external factors, such as the system through which the gas is introduced into the contactor or the fluid dynamic conditions of the agitation of the ozonized solution. For better comprehension, Figure S1 shows the evolution of the utilization coefficient as a function of the pH and dose of ozone. The utilization coefficient (%) is defined as follows:

$$U_{O_3} = \frac{C_{O_3,in} - C_{O_3,out}}{C_{O_3,in}} \times 100 \quad (4)$$

In both cases, two consecutive and distinct steps were observed. In the first step, up to approximately 5 min, it was observed that ozone transferred from the gas phase to the liquid phase, in which ozone becomes a molecular compound in water that previously did not exist. After that, a transitory step occurred, in which the ozone transferred from the gas to the liquid phase is greater than that consumed through self-decomposition and reaction with TiO_2/GAC catalyst. Finally, a stationary

state was reached, in which ozone accumulated in the system reached saturation and a constant value, resulting in an equilibrium between the transferred and consumed ozone.

In Figure S1a, it can be observed that, after reaching saturation, a utilization coefficient of 32% was obtained at pH = 7.0, compared to 19.5% obtained at pH = 3.0. This difference was due to the different solubility that ozone has in water at different pH values, as explained above. The utilization value of 24.8% obtained at pH = 9.0 may be due to the fact that the transferred ozone instead contributes to the accumulation of ozone in the liquid phase; in this case, it would undergo self-decomposition [12]. In the study of the ozone dose effect (Figure S1b), it can be observed that an increase in the ozone dose reduces the efficiency of ozone use. This can be justified largely by the study carried out by Rodriguez et al. [23]. In their study, the degradation of a dye such as rhodamine 6G was evaluated at different pH values and doses of ozone in the presence of activated carbon. The ozone transfer and subsequent consumption was conditioned by parameters, such as pH, which indirectly affect the reactivity of the compound to be oxidized but not the concentration of ozone dose applied.

Von Sonntag and Von Gunten [33] studied the reactivity of aniline oxidation in an ozonation process at different pH values. It was found that, at pH = 6.5, an oxidation kinetic constant of 1.4×10^7 M^{-1} s^{-1} was obtained versus pH = 1.5, where a constant of 5.9×10^4 $M^{-1}s^{-1}$ was obtained. All of this indicates that, at pH = 7.0, the best operating conditions will be obtained (with regards to the chemical reaction of oxidation and transfer of ozone from the gas phase to the liquid).

3.1.2. Aniline Degradation Kinetic Modelling

Modelling of the catalytic ozonation process was carried out to describe the combined action of ozone and TiO_2/GAC composite and to predict and estimate the overall parameters affecting the process of degradation (and, in particular, the mineralization) of aniline. In this section, we propose applying the adaptation of the three-phase mathematical model described by Ferreiro et al. [19], which considers G-L ozone mass transfer, the adsorption process as well as the parallel oxidation that takes place in the liquid phase and the oxidation at the surface of the catalytic material (TiO_2/GAC). The model proposed allows the evolution of the monitored pollutant or total organic carbon (TOC) during the simultaneous oxidation reaction and adsorption process to be calculated. For application of this simultaneous adsorption–oxidation (Ad/Ox) model, it was assumed that:

- The rate of the global ozonation process, or G-L mass transfer rate, coincides with the consumption of ozone in the parallel (liquid and solid) reactive process.
- The oxidation kinetics of aniline in the liquid and in the solid, in terms of TOC, is considered as pseudo-first order.
- For the TiO_2/GAC composite, it was considered a sufficiently porous material for ozone and aniline diffusion mechanisms to take place also in the internal surface of particle.
- The kinetic constant of the aniline oxidation on the solid, also in terms of TOC, includes desorption of degradation compounds.
- The adsorption process is simultaneous to the reaction process on the solid so that its kinetics are strongly affected by the ozonation conditions.

Based on these considerations, Ferreiro et al. [19], for an Ad/Ox process, deduced Equation (5) to express the decrease in contaminant concentration in the liquid in terms of total organic carbon (C_p). The degradation of the pollutant, r_p, should be explained at two levels: in the liquid (r_p^I) and on the activated carbon (r_p^{II}), as a consequence of the oxidative action of the ozone transferred and consumed in the liquid ($N_{O_3}^I$) and on the solid ($N_{O_3}^{II}$), respectively. In addition to the degradation of the pollutant, the elimination due to adsorption is important in the first stages of the process.

$$-\frac{dC_p}{dt} = r_p^I + r_p^{II} + \left(\frac{dC_p}{dt}\right)_{ads} \quad (5)$$

The kinetic parameters of oxidation and adsorption can be expressed as a function of the respective kinetic constants ($k_{c,L}$, $k_{c,S}$, and k_{ads}), ozone concentration, and pollutant, according to the following:

$$r_p^I + r_p^{II} = \left(z^I N_{O_3}^I + z^{II} N_{O_3}^{II}\right) = k_{c,L} \times C_{O_3,L} \times C_p + k_{c,S} \times \frac{C_{O_3,L}}{m} \times M_{CAT} \times Z_p \quad (6)$$

$$\left(\frac{dC_p}{dt}\right)_{ads} = k_{ads} \times \left(Z_{p,\infty} - Z_p\right)^2 \times M_{CAT} \quad (7)$$

In Equation (6), the stoichiometric coefficients z^I and z^{II} express the amount of pollutant (mg TOC per mg of ozone) consumed in the liquid and on the catalyst, respectively. The above equation assumes that the concentration of ozone on the catalyst, $C^*_{O_3,S}$ is in equilibrium with the liquid ozone concentration, $C_{O_3,L}$, and can be expressed as a function of this, according to $C_{O_3,L} = m \times C^*_{O_3,S}$, where m (mg L^{-1})/(mg g^{-1} catalyst) is the slope of the corresponding L-S balance. On the other hand, Z_p is the concentration of total organic carbon adsorbed in the catalyst (mg g^{-1}), M_{CAT} is the concentration of catalyst (g L^{-1}), and $Z_{p,\infty}$ is the amount of total organic carbon adsorbed in the catalytic material at equilibrium (mg g^{-1}), according to the Freundlich equation:

$$Z_{p,\infty} = K_F \times C_p^{1/n} \quad (8)$$

where K_F is a Freundlich constant that indicates the adsorption capacity of the adsorbent (mg g^{-1}) (L $mg^{-1})^{1/n}$ and n describes the adsorption intensity. Values of n between 2 and 10 indicate good adsorption intensity [34].

In a semi-continuous process in which an ozone flow is continuously injected, the concentration of ozone in the liquid, C_{O_3}, is assumed to be constant during the reaction [23]. This assumption can be used to define the apparent first-order kinetic constants—k_{oxL} in the liquid and k_{oxS} over the catalyst—to describe the degradation of the aniline, in terms of TOC (min^{-1}). Consequently, the overall pollutant concentration variation (Equation (5)) can be written as follows:

$$-\frac{dC_p}{dt} = k_{oxL} \times C_p + k_{oxS} \times M_{CAT} \times Z_p + k_{ads} \times \left(Z_{p,\infty} - Z_p\right)^2 \times M_{CAT}, \quad (9)$$

where C_p is the concentration of the pollutant (TOC) at a given time t (mg L^{-1}), Z_p is the concentration of total organic carbon adsorbed onto the catalyst (mg g^{-1}), M_{CAT} is the concentration of catalyst (g L^{-1}), $Z_{p,\infty}$ is the amount of total organic carbon adsorbed in the composite at equilibrium (mg g^{-1}), k_{oxL} is the first-order kinetic constant due to the oxidation of aniline in the liquid (min^{-1}), k_{oxS} is the pseudo-first-order kinetic constant due to oxidation on the catalytic material (min^{-1}), and k_{ads} is the aniline adsorption constant (g mg^{-1} min^{-1}). The combination of Equations (8) and (9) provides a description of the variation in the pollutant concentration in the system from the determination of the kinetic parameters (k_{oxL}, k_{oxS}, and k_{ads}) and the equilibrium parameters (K_F and n).

3.1.3. Evaluation of Operating Conditions for Model Validation

Operational parameters such as pH, ozone concentration, or the dose of catalyst used have a considerable effect on the efficiency of the removal of aniline using catalytic ozonation processes with TiO_2/GAC catalyst. Using the Ad/Ox model described above, it is possible to explain the effects of the different parameters, such as the behaviour of the ozone or the catalyst dosage. In Figure 3, the evolution of aniline degradation is shown, as well as the mineralization under various pH values (3.0, 5.0, 7.0, and 9.0), ozone concentrations at the inlet (3.7, 5.4, 11.3, and 20.1 mg L^{-1}), and catalyst doses (1.6, 3.3, 6.6, and 13.3 g L^{-1}).

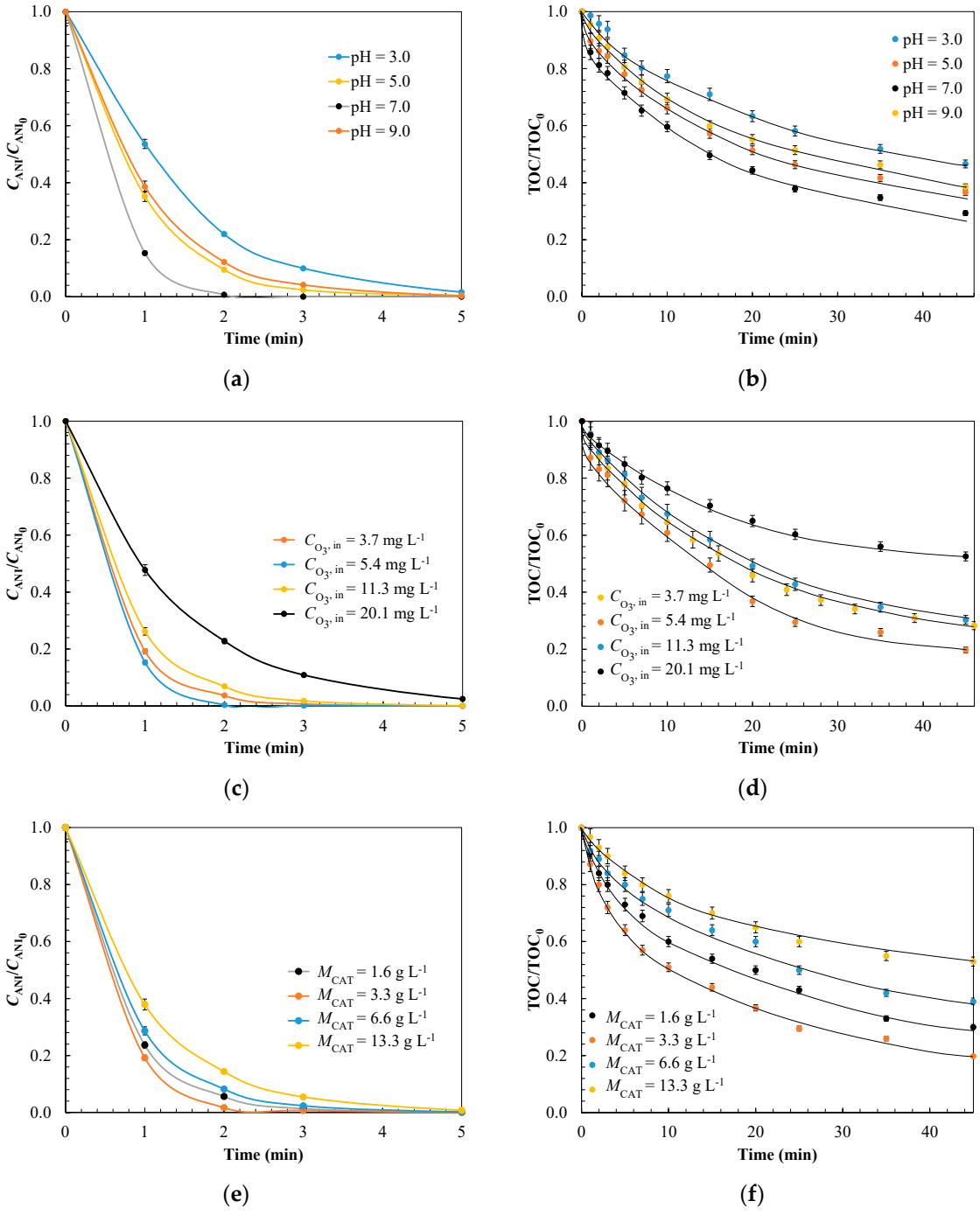

Figure 3. Effect of operating conditions on catalytic ozonation with TiO_2/GAC: (**a**) pH [1], (**c**) inlet ozone concentration [2], and (**e**) mass of TiO_2/GAC catalyst in the aniline removal [3] and (**b**) [1], (**d**) [2] and (**f**) in TOC (mineralization), showing experimental and modelled profiles fitted to the Ad/Ox process [3]. Experimental conditions: Q_G = 4 L min^{-1}; T = 18.0 °C; P = 1 atm; V_{reac} = 1.5 L; (*Agitation*) = 60 rpm. [1] $C_{O_3,in}$ = 5.4 mg L^{-1}, M_{CAT} = 3.3 g L^{-1}; [2] pH = 7.0, M_{CAT} = 3.3 g L^{-1}; [3] pH = 7.0, $C_{O_3,in}$ = 5.4 mg L^{-1}.

The pH has a significant effect on the catalyst, as it directly affects the pathway through which the ozone acts on the organic compound. Figure 3a,b shows that the best conditions for the effective removal of aniline are present at a neutral pH of 7.0. The change in basicity associated with pollutant removal at that pH, or specific basicity loss, is optimal [35]. In addition, it was observed that those experiments conducted at slightly alkaline pH (pH = 9.0) obtained a higher oxidation rate because, under these conditions, the indirect pathway for hydroxyl radical generation is promoted by the

interaction between ozone and the TiO_2/GAC catalyst. On the other hand, at acidic pH (pH = 3.0), a more limited oxidation and mineralization rate was observed because, at this pH value, the attack through the molecular pathway between ozone and aniline is mostly promoted [36,37]. Although this pathway is more selective than the radical one, the oxidation power of molecular ozone (2.07 V) is lower than that of the hydroxyl radicals (2.80 V) [28].

On the other hand, the dose of ozone in the catalytic ozonation reaction system is a critical parameter for the degradation and mineralization of aniline. In Figure 3c,d, it is shown that, with an ozone dose of 5.4 mg L^{-1}, the highest aniline mineralization was achieved, with a value of 80.2%. However, upon increasing the ozone dose considerably (to 20.1 mg L^{-1}), a negative effect was obtained as opposed to the generation of a larger amount of hydroxyl radicals. This was due to the fact that, on the surface of the TiO_2/GAC catalyst, instead of generating hydroxyl radicals for the degradation of the organic compound, other species were generated, such as hydroperoxyl radicals—which have a lower oxidation potential (1.70 V) than hydroxyl radicals (2.80 V) or ozone (2.07 V) [38]. Moreover, a very high ozone dose (20.1 mg L^{-1}) could transform the basic sites into acidic sites, as the oxidation of the carbonaceous support can generate acidic groups such as lactones or carboxylic acid, which could negatively influence the adsorptive properties of the TiO_2/GAC composite itself [39]. This last aspect will be analysed in detail later on.

In Figure 3e,f, the effect of the catalyst dose on the aniline removal rate is shown, providing information on the optimal use of the TiO_2/GAC material. An increase in catalyst dosage led to increased degradation and mineralization of the aniline, with a favourable dosage of 3.3 g L^{-1}, where mineralization was close to 80% and complete degradation of the aniline was achieved in less than 10 min. In general, a higher catalyst dose increases the number of active sites on the surface of the composite, thus facilitating the further decomposition of ozone into hydroxyl radicals [40]. However, above a certain critical value, a decrease in TOC removal was observed, which may be due to the adsorption of a higher proportion of pollutant on the catalyst, thus reducing the catalytic effect [38] in favour of the adsorption. This indicates that a small amount of catalyst is sufficient to induce a radical chain reaction that appears to be more effective on the dissolved than adsorbed pollutant. Moussavi and Khavanin [41] studied the effect of the dose of activated carbon in a catalytic ozonation process for the removal of phenol. It was observed that, from the optimal dose of catalyst, no further improvement in mineralization was observed, as with the TiO_2/GAC composite. Consequently, it was concluded that there is an optimal dose of catalyst, which changes depending on the type of catalyst, the organic compound to be eliminated, the operational conditions of the reaction, and the desired cost-effectiveness.

The TOC removal kinetics was fitted to the model proposed in Section 3.1.2 by solving Equations (8) and (9). Before analysing the results obtained from the Ad/Ox model, it was verified that under the operating conditions studied the assumption of control of the chemical reaction during catalytic ozonation was satisfied.

The control regime was verified through the U_{O_3} profiles shown in Figure S2. It can be seen at the lowest ozone doses ($C_{O_3,in}$ = 3.7 mg L^{-1}), in the initial instants, the ozone concentration in the gaseous phase is practically zero (U_{O_3} = 100%). This indicates that the process is controlled by the mass transfer. However, after 4 min it changes to be controlled by the chemical reaction, once $C_{O_{3,L}}$ starts rising. For resolution of the TOC removal kinetics, the calculation tool Scilab® was used, with which the corresponding adjustment to the experimental data was simulated to obtain the adsorption and ozonation kinetics constants during the removal of aniline with the previous determination of equilibrium adsorption constants. As for the initial conditions of the dependent variables involved in the differential equation, at the initial time, an aniline concentration of 20.0 mg L^{-1} was considered, corresponding to an initial TOC concentration of $C_{p,0}$ = 12.50 mg L^{-1} and the TiO_2/GAC free of aniline or other organics ($Z_{p,0}$ = 0.0 mg g^{-1}). C_p^* vs. t modelled profiles were fitted to the experimental ones

(of N values), in order to minimize the weighted standard deviation, σ, given by Equation (10). Thus, the estimated values of k_{ads}, k_{oxL}, and k_{oxS} are listed in Table 3 [42]:

$$\sigma = \sqrt{\frac{\sum_{i=1}^{N}\left(\frac{(C_p - C_p^*)}{C_p}\right)^2}{N-1}} \quad (10)$$

Table 3. Summary of the adsorption and oxidation kinetic constants for the mineralization of wastewater containing aniline using Norit® GAC 1240 Plus and TiO_2/GAC composite by catalytic ozonation.

Catalyst Comparison		
Kinetic Parameter	**Norit® GAC 1240 Plus** [1,2]	**TiO_2/GAC** [1,2]
$k_{ads} \times 10^{-4}$, g mg^{-1} min^{-1}	2.4	3.5
$k_{oxL} \times 10^{1}$, min^{-1}	8.1	5.9
$k_{oxS} \times 10^{1}$, min^{-1}	0.0030	2.3
σ	0.050	0.046

TiO_2/GAC Composite Analysis				
Kinetic Parameter	**Effect of pH**			
	3.0	**5.0**	**7.0**	**9.0**
$k_{ads} \times 10^{-4}$, g mg^{-1} min^{-1}	3.6	3.1	2.9	2.5
$k_{oxL} \times 10^{1}$, min^{-1}	3.4	6.5	8.3	8.6
$k_{oxS} \times 10^{1}$, min^{-1}	0.20	1.1	1.2	0.90
σ	0.061	0.053	0.059	0.048
Kinetic Parameter	**Effect of Ozone Inlet Concentration, mg L^{-1}**			
	3.7	**5.4**	**11.3**	**20.1**
$k_{ads} \times 10^{-4}$, g mg^{-1} min^{-1}	3.2	3.5	2.9	1.8
$k_{oxL} \times 10^{1}$, min^{-1}	4.2	5.9	8.3	11.5
$k_{oxS} \times 10^{1}$, min^{-1}	1.5	2.3	1.2	0.50
σ	0.052	0.046	0.057	0.045
Kinetic Parameter	**Effect of Catalyst Dose, g L^{-1}**			
	1.6	**3.3**	**6.6**	**13.3**
$k_{ads} \times 10^{-4}$, g mg^{-1} min^{-1}	1.8	3.5	4.4	8.4
$k_{oxL} \times 10^{1}$, min^{-1}	3.8	5.9	2.2	1.0
$k_{oxS} \times 10^{1}$, min^{-1}	1.9	2.3	1.5	0.90
σ	0.054	0.046	0.055	0.052

[1] Experimental conditions: Q_G = 4 L min^{-1}; $C_{O_3,in}$ = 5.4 mg L^{-1}; pH_0 = 7.0; M_{CAT} = 3.3 g L^{-1}; T = 18.0 °C; P = 1 atm; V_{reac} = 1.5 L; (*Agitation*) = 60 rpm. [2] Freundlich equilibrium parameters: K_F = 33.07 (mg g^{-1})(L mg^{-1})$^{1/n}$, n = 2.39 for Norit® GAC 1240 Plus and K_F = 44.02 (mg g^{-1})(L mg^{-1})$^{1/n}$, n = 3.97 for TiO_2/GAC composite.

The Freundlich parameters of the catalytic materials tested are given in Table 3, which were obtained experimentally in the previous adsorption tests. The C_p values had an acceptable fit to the Ad/Ox model with a weighted standard deviation of $\sigma \cong 0.05$ for the mineralization kinetics.

In Table 3 it was observed that the k_{oxS} constant was lower than k_{oxL}. This is because in the solid involved an oxidation reaction in conjunction with the adsorption phenomena in parallel. From the comparison of the catalytic ozonation with Norit® GAC 1240 Plus activated carbon and TiO_2/GAC composite, it can be seen that the TiO_2/GAC catalysts kinetically favour adsorption, with $k_{ads} = 3.5 \times 10^{-4}$ g mg^{-1} min^{-1}, compared to commercial carbon ($k_{ads} = 2.4 \times 10^{-4}$ g mg^{-1} min^{-1}). Its higher adsorption capacity, rather than the specific surface (S_{EXT} = 298.9 m^2 g^{-1})—which is very similar to that of commercial activated carbon (S_{EXT} = 224.4 m^2 g^{-1})—explains this behaviour, despite the fact that TiO_2/GAC has a 25% larger external surface, as seen in the Material and Methods

section [43]. The adsorption properties of metal oxides, such as TiO_2, deposited onto GAC, appear to also enhance the catalytic activity. Other authors [37,44] have highlighted that metal oxides have a high adsorption capacity, which is due to ligand exchange reactions that provide strong bonds between the ionized species and the active site of the metal oxide surface. The increase in the oxidation kinetic constant in the solid, from a value of $k_{oxS} = 0.003 \times 10^1$ to 2.3×10^1 min^{-1}, in the TiO_2/GAC composite is remarkable. This increase is due to the contribution of TiO_2 in the activated carbon, improving its reactivity and the number of active sites on the catalyst. The deposited TiO_2 is responsible for efficiently decomposing the ozone, producing $HO^{\bullet}$ radicals. Other properties, such as pore volume, porosity, pore size distribution, and, particularly, the presence of active sites on the surface (e.g., Lewis acid sites, which are responsible for the catalytic reactions), may be responsible for this increase in k_{oxS} [45]. Acidity or basicity, for example, is key to surface properties. Furthermore, the hydroxyl groups, which are present on all surfaces of the metal oxides, are dependent on the deposited metal oxide [39]. Valdés and Vega [45] studied the effect of the chemical structure of various active carbons on the catalytic activity for the generation of hydroxyl radicals, where they suggested that the presence of iron metal ions played an important role in the decomposition of ozone and hydrogen peroxide towards the generation of radicals. Those carbons with more basic surface functionalities led to a higher radical generation and, consequently, to a higher catalytic activity.

Authors such as Orge et al. [46] and Kasprzyk-Hordern et al. [38] have suggested that the variability of surface properties and interactions between the catalyst and ozone with organic pollutants results in different reaction mechanisms, derived from two main types: Langmuir–Hinshelwood (LH) or modified Eley–Rideal (ER).

The LH stage consists of adsorption, surface reaction, and subsequent desorption [28]:

Adsorption of ozone onto every site, *S*, of GAC surface:

$$O_3 + S \overset{K_{LH1}}{\rightleftarrows} O = O - O - S \tag{11}$$

$$O = O - O - S \overset{k_{LH2}}{\rightarrow} O - S + O_2 \tag{12}$$

Adsorption of aniline:

$$C_6H_5NH_2 + S \overset{K_{LH3}}{\rightleftarrows} C_6H_5NH_2 - S \tag{13}$$

Surface reaction and desorption of oxidation products:

$$\frac{21}{2}O - S \; + \; C_6H_5NH_2 - S \overset{k_{LH4}}{\rightarrow} NO_3^- + 2CO_2 + \frac{7}{2}H_2O + 2S \tag{14}$$

The other mechanism (modified ER), proposed by Beltran et al. [44], is specific for metal oxides supported on activated carbon materials and consists of an adsorption stage on the GAC, together with the assumptions of the modified ER mechanism. In this case, these stages are: (i) the adsorption of aniline onto the TiO_2/GAC composite, (ii) the reaction stage between the adsorbed aniline and the ozone, and (iii) the irreversible ozonation reaction of adsorbed pollutant.

Adsorption of aniline on the GAC active sites:

$$C_6H_5NH_2 + S \overset{K_{ER1}}{\rightleftarrows} C_6H_5NH_2 - S \tag{15}$$

Adsorption of aniline on the TiO_2 active sites:

$$C_6H_5NH_2 + S' \overset{K_{ER2}}{\rightleftarrows} C_6H_5NH_2 - S' \tag{16}$$

where S′ represents any active site on the TiO_2.

Reaction between ozone and adsorbed aniline on TiO_2 active sites:

$$\frac{41}{2}O_3 + C_6H_5NH_2 - S' \overset{k_{ER3}}{\Rightarrow} 6CO_2 + \frac{7}{2}H_2O + O_2 + NO_3^- + S' \quad (17)$$

In this last mechanism, it was assumed that the CO_2 generated corresponds to that resulting from complete mineralization. Overall, it can be concluded that the removal of aniline is due to an adsorption process on the GAC and to the catalytic ozonation itself, which takes place in the active centres of the TiO_2 metal oxide. Based on the values of the k_{oxS} and k_{oxL} constants obtained from the three-phase model, it is possible to qualitatively determine the predominant mechanism (LH or modified ER). An intensification of the k_{oxS} constant due to the presence of TiO_2 metal oxide against the k_{oxL} constant indicates the predominance of the modified ER mechanism. In contrast, negligible values of the k_{oxS} constant compared to the k_{oxL} constant indicate the predominance of the LH mechanism. Taking into account the mechanical aspects of the reaction system, the effect of operational variables, such as pH, ozone dosage, and TiO_2/GAC catalyst loading were analysed.

Regarding the effect of pH, due to the surface properties of the composite, it was observed that the adsorption constant increased under more acidic pH values, while under alkaline pH values, the quantity of aniline removed decreased. This is due to the speciation of the aniline, with pK_a = 4.61 [47], and the character of the surface of the composite through the zero loading point (pH_{pzc} = 6.4). The TiO_2/GAC composite, at a pH below 6.4, develops a negative charge on its surface; below pH = 4.61, it will mostly be in ionic form, favouring adsorption. On the other hand, under alkaline pH, the affinity between the aniline and the surface of the material is weak and adsorption is limited. Similarly, Shahamat et al. [48], in a catalytic ozonation process in which a carbon nanocomposite was used for the removal of phenol, observed the same behaviour at a pH between pH_{pzc} and pK_a. The oxidation constant in the liquid, k_{oxL}, increased from a value of 3.4×10^1 to 8.6×10^1 min^{-1}, due to the fact that, under alkaline conditions, the radical pathway in which ozone directly attacks the OH^- generating radicals $HO^\bullet$ is favoured, according to [49]:

$$O_3 + OH^- \rightarrow O_3^{\bullet -} + HO^\bullet, \quad (18)$$

$$O_3^{\bullet -} \rightarrow O^\bullet + O_2, \quad (19)$$

$$O^{\bullet -} + H^+ \rightarrow HO^\bullet \quad (20)$$

As for k_{oxS}, the maximum value observed was 1.2×10^1 min^{-1} at pH = 7.0. This increase was due to the contribution that TiO_2 metal oxide provides to the GAC, thus improving the capacity of transforming ozone into hydroxyl radicals. According to Roshani et al. [50], the surface charge and the capacity of the TiO_2/GAC composite to transfer electrons to the ozone are factors that affect the elimination of TOC. Operating at a pH of 7.0, favourable conditions allow for a positive interaction between the ozone and TiO_2 metal oxide, which allows for the decomposition of ozone and, thus, the generation of a greater number of $HO^\bullet$ radicals in sufficient quantity to oxidize the organic compounds adsorbed on the surface of the GAC. According to Nawrocki and Kasprzyk-Hordernb [51], considering the type of radicals formed on TiO_2 nanoparticles in the presence of ozone, it was concluded that catalytic ozonation was more effective at a pH close to pH_{pzc}. Under these conditions, the presence of neutral hydroxyls are responsible for the formation of the hydroxyl radical.

For the effect of the ozone dose, it was observed that the use of a low ozone dose ($C_{O_3,in}$ = 3.7 mg L^{-1}) led to a mineralization yield of 69%, as the amount of hydroxyl radicals generated was low. Taking into account the distribution of the kinetic constants obtained (Table 3), when the dose is insufficient, the adsorbent effect is enhanced but not the oxidation of the organic pollutant. On the other hand, with a high dose ($C_{O_3,in}$ = 20.1 mg L^{-1}), ozone accumulates in the system, favouring the generation of the less reactive perhydroxyl radical ($HO_2^\bullet$), according to [49]:

$$O_3 + HO^\bullet \rightarrow O_2 + HO_2^\bullet \quad (21)$$

It seems evident that moderate concentrations favour the adsorption kinetics and result in a sufficient generation of hydroxyl radicals on the surface of the catalyst. A dose of 5.4 mg L^{-1} ensures that the aniline is adsorbed rapidly over the GAC (k_{ads} = 3.5 × 10^{-4} g mg^{-1} min^{-1}) and, at the same time, maximizes oxidation at the solid level (k_{oxS} = 2.3 × 10^{1} min^{-1}), where TiO_2 plays an important role. The action of ozone on the adsorbed aniline, according to the modified ER mechanism (see Equation (17)), appears to be the dominant mechanism in this case and responsible for the high k_{oxS} value.

Concerning the effect of catalyst loading, it was observed that, by increasing the dose from 1.6 to 13.3 g, the adsorption constant increased from 1.8 × 10^{-4} to 8.4 × 10^{-4} g mg^{-1} min^{-1}. A higher quantity of adsorbed organics and ozone is to be expected when increasing the amount of catalyst but does not result in further destruction of the aniline. It can be observed that high doses of catalyst lead to a predominance of surface oxidation reactions, as a result of increased TiO_2/GAC active sites and an increased amount of adsorbed contaminant [36]. However, the most favourable values were produced with an intermediate amount of catalyst (k_{oxS} = 2.3 × 10^{1} min^{-1}). The negative effect became increasingly evident as the amount of catalyst increased, which was related to a change in the mechanism of the oxidation processes at the solid level. According to the assumption made in Section 3.1.3, a transition from the modified ER to the LH mechanism should take place. In effect, with small amounts of catalyst, a moderate amount of contaminants was adsorbed—preferably on TiO_2—through non-associated hydroxyl groups [52] or S' sites (Equation (17)) with favourable incidence in the increase of k_{oxS} and consequently in the degradation of the contaminant. An increase in the amount of catalyst led to a greater proportion of the contaminant being adsorbed, resulting in the occupation of S sites and participation of slow rate reactions (such as that shown in Equation (14)), with a subsequent decrease in k_{oxS}. A decrease in the degradation of the aniline at the liquid phase as k_{oxL} = 1.0 × 10^{1} min^{-1} decreased and the lower proportion of contaminant in the liquid were other negative effects associated with an increase in the amount of catalyst [38]. Moderate amounts of catalyst (3.3 g L^{-1}) favoured oxidation at the solid and liquid level, obtaining the highest mineralization (80% TOC removal) in 45 min.

3.2. Physicochemical Surface Characterization of Spent-Granular Activated Carbon

In order to verify the lower generation of hydroxyl radicals when a high catalyst dose was used and that the aniline would be oxidized under very poor oxidation conditions, an analysis of the physicochemical properties of the TiO_2/GAC composite used was carried out, as shown in Table 4.

Table 4 shows a decrease of the specific surface of the TiO_2/GAC composite of the experiment performed with a catalyst load of 13.3 g L^{-1} from 985.0 to 901.2 m^2 g^{-1}. The pore volume was also reduced, but the physical properties were practically unchanged with a catalyst dose of 3.3 g L^{-1}. Considering the importance of the adsorption stages contemplated in the Ad/Ox model, the necessary equilibrium of reactions at the liquid and solid level should not be broken. This balance is broken when the catalyst dose is increased, with negative effects on the degradation of the contaminant being key in the optimization of the process.

Concerning the chemical properties (e.g., the point of zero charge), ozone appeared to affect them by a small amount. The carbonaceous support lost active basic sites while the concentration of the acidic functional groups increased, leading to a reduction in adsorption capacity over long periods [53].

Table 4. Physicochemical properties of pristine and spent TiO_2/GAC in aniline ozonation with different catalyst doses. Experimental conditions: Q_G = 4 L min^{-1}; $C_{O_3,in}$ = 5.4 mg L^{-1}; pH = 7.0; T = 18.0 °C; P = 1 atm; V_{reac} = 1.5 L; (*Agitation*) = 60 rpm.

Property	Pristine TiO_2/GAC	Spent TiO_2/GAC	
		M_{CAT} = 3.3 g L^{-1}	M_{CAT} = 13.3 g L^{-1}
S_{BET}, m^2 g^{-1}	985.0	980.4	901.2
S_{ext}, m^2 g^{-1}	298.9	289.1	267.5
V_T, cm^3 g^{-1}	0.45	0.39	0.32
V_μ, cm^3 g^{-1}	0.29	0.25	0.20
V_M, cm^3 g^{-1}	0.16	0.14	0.12
V_M/V_T, %	35.2	35.9	37.5
V_μ/V_T, %	64.8	64.1	62.5
D_P, Å	33.9	33.0	29.3
pH_{pzc}	6.4	6.2	6.3

Moreover, Figure 4 shows FTIR spectra of the non-ozonized and ozonized TiO_2/GAC catalyst using a 13.3 g L^{-1} load, in order to confirm the presence of compounds that verify the previous hypothesis. According to Figure 4, it was observed that most of the spectral bands corresponded to organic compounds, highlighting the band from 3300 to 3500 cm^{-1} (–OH stretching), which is due to the presence of water in the sample during preparation. The 500 cm^{-1} spectral band (Ti–O stretching) corresponded to the presence of TiO_2 deposited on the GAC [54]. The main spectral modifications, when comparing the sample of the non-ozonized composite and the ozonized one, were detected in the emergence of the 790 cm^{-1} band. The accumulation of intermediate species, such as oxamic acid, and subsequent sorption in the solid explain this FTIR sorption band [55]. The peak near to 2800 cm^{-1} would correspond to aldehyde groups, such as formaldehyde or acetaldehyde, and strongly depended on the ozone dose, adsorbed on the catalyst due to the opening of the aromatic ring [56], while another band at 1102 cm^{-1} was due to the superoxide radical [57].

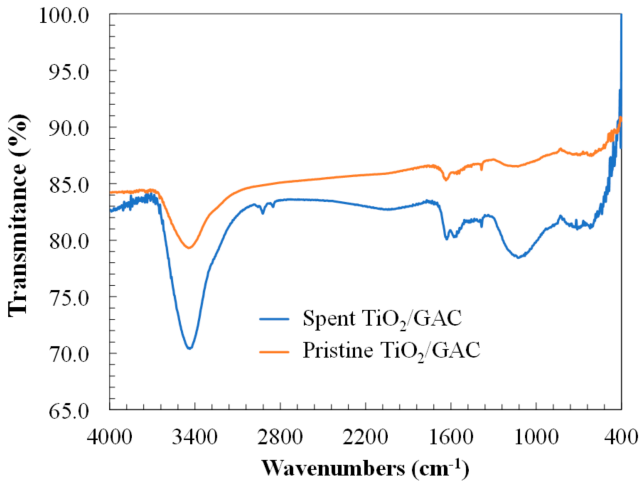

Figure 4. FTIR spectra of pristine and spent TiO_2/GAC composite in the aniline catalytic ozonation. Experimental conditions: Q_G = 4 L min^{-1}; $C_{O_3,in}$ = 5.4 mg L^{-1}; pH = 7.0; M_{CAT} = 13.3 g L^{-1}; T = 18.0 °C; P = 1 atm; V_{reac} = 1.5 L; (*Agitation*) = 60 rpm.

3.3. Degradation Pathway Approach

In order to provide more detail on the types of intermediates formed when increasing the dose of catalyst, other physical–chemical parameters, such as turbidity, were analysed. In Figure 5, the effect of the catalyst dose on turbidity is shown. Solid particles or high molecular weight insoluble degradation products usually cause turbidity [58]. The experiment with the highest amount of catalyst

(13.3 g L^{-1} TiO_2/GAC catalyst), with an ozone dose of 5.4 mg L^{-1} and a neutral pH, led to the highest turbidity, with a turbidity of 17 NTU after a reaction time of 45 min. However, with a catalyst dose of 3.3 g L^{-1}, the lowest turbidity was produced, corresponding to the highest mineralization observed. Consequently, the higher turbidity could be associated with the formation of more recalcitrant intermediate products.

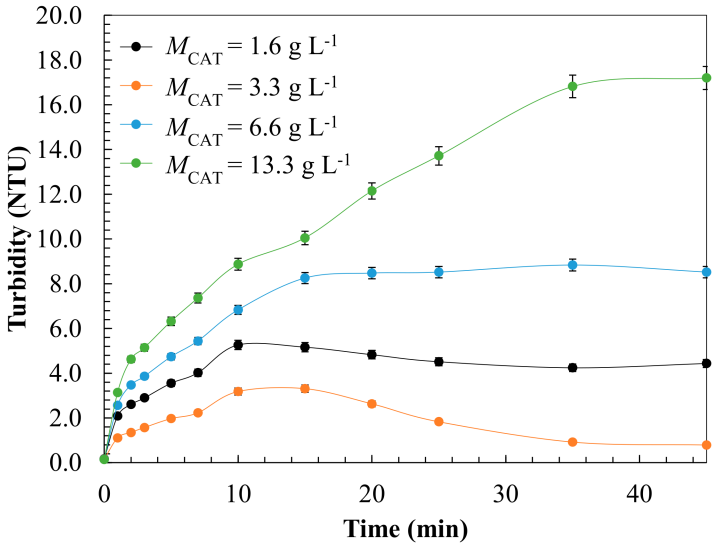

Figure 5. Effect of TiO_2/GAC catalyst dosage on turbidity during catalytic ozonation of aniline containing wastewater. Experimental conditions: Q_G = 4 L min^{-1}; $C_{O_3,in}$ = 5.4 mg L^{-1}; pH = 7.0; T = 18.0 °C; P = 1 atm; V_{reac} = 1.5 L; (*Agitation*) = 60 rpm.

Orge et al. [22] have highlighted oxalic and oxamic acid among the reaction products of aniline with the highest resistance to degradation. Figure 6 shows the results obtained from the identification of aniline, oxamic acid, and oxalic acid at the initial time, after decomposition of the aniline (≈5 min), and after a sufficiently long reaction time. Figure 6d shows the chromatogram obtained at zero time (peak 1) with a retention time of 8.21 min, which was assigned to aniline. After the catalytic ozonation reaction had progressed for 5 min, the peak of the aniline (1) decreased but others appeared, which persisted until sufficiently long reaction times (30–40 min). The mass spectra of the identified peaks are shown in Figure 6a–c. These peaks were assigned to oxalic (2, 1.80 min) and oxamic acid (3, 2.65 min), corresponding to two degradation intermediates formed during the ozonation of the ozone aniline [59].

Oxalic acid under conditions of low hydroxyl radical generation as well as its conjugate base are stable degradation intermediates for a wide variety of organic contaminants, such as pesticides. The accumulation of this refractory compound in the reaction system is due to its very low oxidation constant ($k < 0.04$ M^{-1} s^{-1} at pH values above 5.0), compared to that of other aniline oxidation products such as hydroquinone ($k = 2.3 \times 10^6$ M^{-1} s^{-1} at pH = 7.0) [33,60]. On the other hand, oxamic acid is another compound present in the degradation of aniline that, under poor oxidation conditions, shows high refractoriness to ozonation [61].

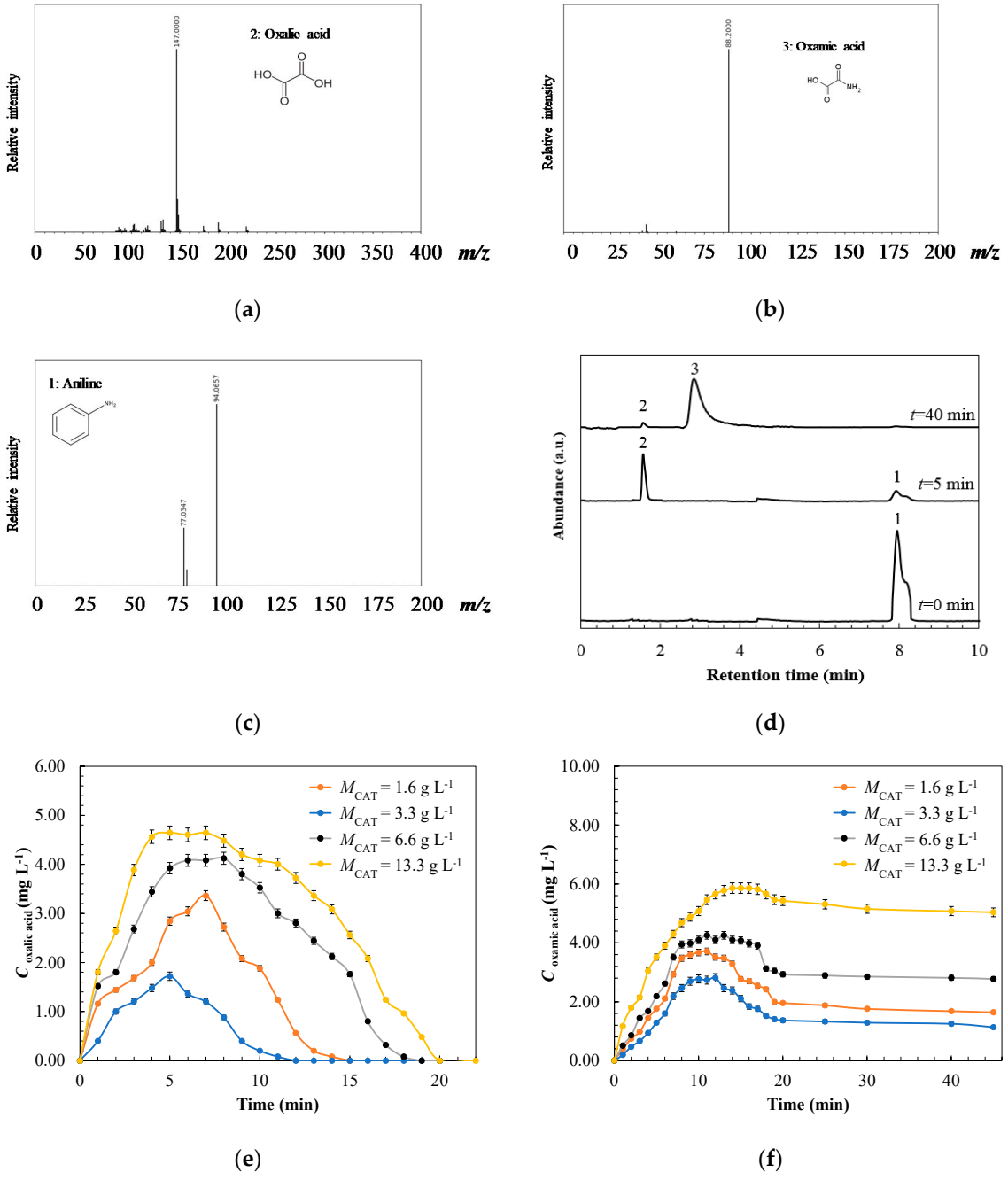

Figure 6. Analysis of some by-products formed during the TiO_2/GAC ozonation of aniline: (**a**–**c**) mass spectrometry (MS) of the aniline at different ozonation times, (**d**) liquid chromatography (LC) of the aniline and representative ozonation by-products, and (**e**,**f**) effect of catalyst dosage on the evolution of oxalic and oxamic acid during ozonation. Experimental conditions: Q_G = 4 L min^{-1}; $C_{O_3,in}$ = 5.4 mg L^{-1}; pH = 7.0; T = 18.0 °C; P = 1 atm; V_{reac} = 1.5 L; (*Agitation*) = 60 rpm.

Figure 6e,f show the evolution of the concentration of oxamic and oxalic acid for different doses of catalyst. For both acids and for all doses of catalyst studied, a continuous increase corresponding to the accumulation phenomenon was observed during the first 5 min. Then, coinciding with the primary degradation of the aniline (Figure 3e), a maximum was reached, which was higher with an increased catalyst dose. The increase in turbidity observed in Figure 5 at any catalyst dose studied is coincident with that of both acids. The relationship between oxalic acid and turbidity is evident, as well as the amount associated with the mechanism change from modified ER to LH. A Langmuir–Hinshelwood

(LH) type oxidative mechanism was dominant, with high amounts of TiO_2/GAC (6.6 or 13.3 g L^{-1}), promoting oxidation products such as oxalic acid [22]. Concerning the evolution of oxamic acid, the initial accumulation was slower, reaching its maximum 7 min later than that observed for oxalic acid. Unlike oxalic acid, oxamic acid could not be removed, explaining the flat tailing observed in the TOC profiles in Figure 3f. In these cases, the hypothesis of a dominant reactive mechanism of type LH at the surface with very low reaction rate (k_{oxS}) seems evident. This situation also led to the high occupation of active centres with a decrease in the radical concentration in the liquid and subsequent decrease in k_{oxL}. Authors such as Faria et al. [61] have reported a similar result during the removal of oxalic and oxamic acid via catalytic ozonation using active carbon. Furthermore, it has been reported that, at neutral pH, oxamic acid is mainly present as a zwitterion ($^{-}OOC—CONH^{3+}$), which is highly hydrophilic and stable in water. The C–H bonds explain its low reactivity towards hydroxyl radicals, and although it is possible to mineralize it completely (according to Legube and Leitner [14]), it requires a hydroxyl radical concentration approximately 100 times higher than that needed for other organic compounds with the same functional group. Thus, the persistence of oxamic acid in the liquid phase can explain the observed turbidity increase.

Due to the catalytic ozonation process in which the aniline was degraded, some degradation intermediates were formed. Using liquid chromatography (LC), higher concentration degradation products, such as nitrobenzene, phenol, catechol, o-benzoquinone, 1,2,3-benzenetriol, p-benzoquinone, and muconic acid, were detected excluding oxamic and oxalic acid. Other organic compounds, which were detected at lower concentrations, could not be identified. In this section, only the first intermediates (C_6) are included, in an attempt to determine the beginning of the first degradation routes. Many of these degradation products showed up in the solution within the first 5 min, through the change from a non-coloured solution to another with reddish, brown, and yellow colouring [6,62,63]. In Figure 7, three cases with the same mass of TiO_2/GAC (3.3 g L^{-1}) were selected, representative of the different experimental conditions studied. Among them, an adverse situation was selected with a low generation of hydroxyl radicals at pH = 3.0, as well as another with an excess of oxidant of 20.1 mg L^{-1}—which was ineffective due to the low mineralization achieved—and, finally, with the favourable conditions indicated in the previous section. For additional information, Figures S3 and S4 show the concentrations of each intermediate in terms of TOC. In Figure S4c, it can be observed that the amount of unknown TOC after 5 min of reaction was 5.9 mg L^{-1}.

According to Figure 7, the two possible degradation routes can be differentiated, according to the involvement of the direct and radical ozone pathways. In addition, it was observed that the rupture of the aniline molecule occurred in the bond between the benzene ring and the amino group (—NH_2). Other authors, such as Villota et al. [64] and Von Sonntag and Von Gunten [33], have also observed this same rupture.

In Figure 7a, it can be observed that the direct attack of ozone could be responsible for the high selectivity towards the formation of dihydroxy aromatic rings, such as catechol or 1,2,4-benzenetriol, through ortho-, meta-, and para-substituted oxidation pathways and electrophilic substitutions [65]. However, the carboxylic acids or muconic acid detected later (after about 10 min of reaction) were more refractory to direct ozone attack, which explains the 40% mineralization observed after a reaction time of 20 min [66].

However, the results in Figure 7b show a different behaviour, in which the aniline was degraded by another mechanism—attributed to the radical pathway. In this case, we note the presence of nitrobenzene. According to Brillas et al. and Tolosana-Moranchel et al. [67,68], the presence of nitrobenzene could be due to the high selectivity of the hydroperoxyl radical, compared with the hydroxyl radical, to the amino group, which strongly favours its conversion to a nitro group. Despite the last point, considering the radical species generated from direct interaction with TiO_2/GAC, Sanchez et al. [69] suggested that the hydroxyl radical is responsible for abstracting hydrogen from the amino group and then substituting it with an iminium radical, thus generating nitrobenzene. The generation of nitrobenzene could explain the low reactivity and inefficiency observed when using

a high dose of ozone. With respect to the presence of phenol or p-benzoquinone, Commninellis and Pulgarin [70] attributed it to hydroxylation reactions of these benzene structures with hydroxyl groups.

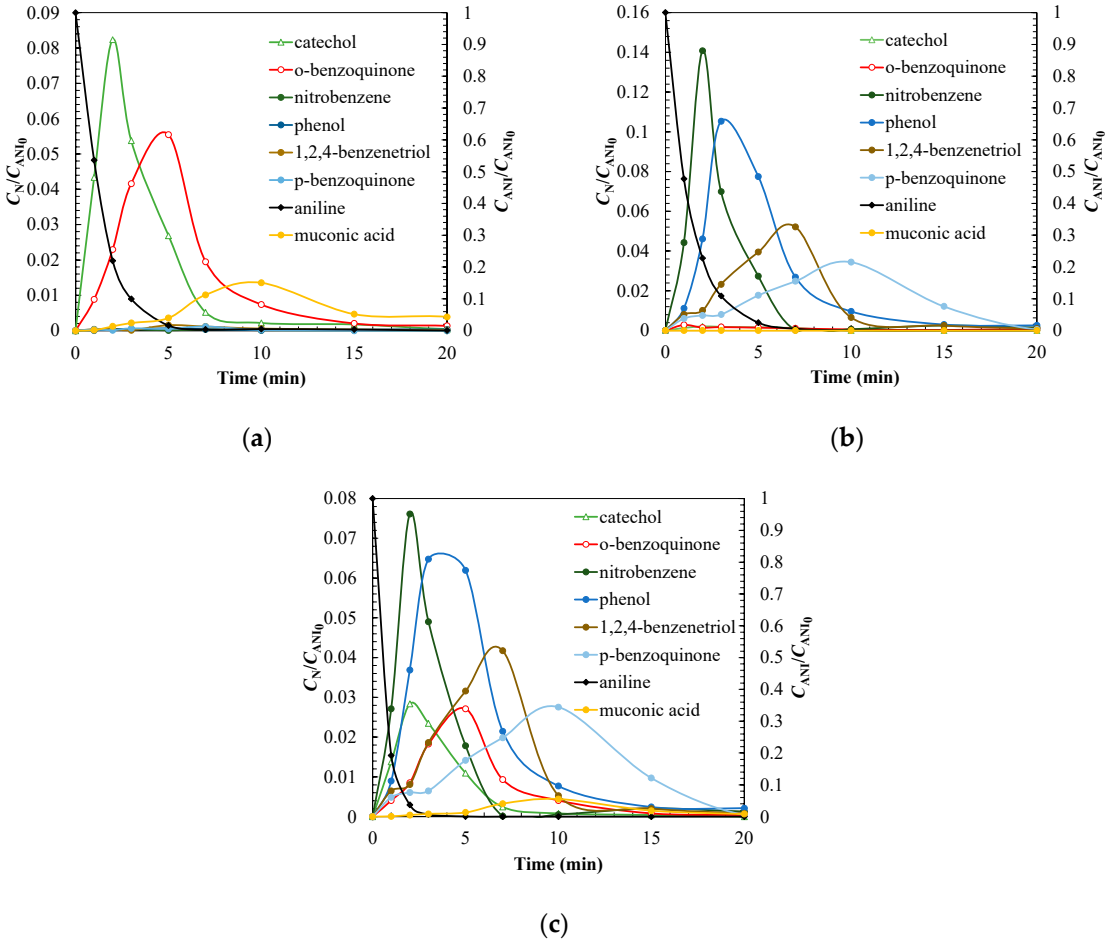

Figure 7. Analysis of the main intermediates in the aniline catalytic ozonation with TiO_2/GAC excluding oxalic and oxamic acid in different cases: (**a**) molecular attack of ozone at pH = 3.0, (**b**) ozone in excess and dominance of radicalary attack (pH = 7.0 and ozone dose of 20.1 mg L^{-1}), and (**c**) most favourable conditions (pH = 7.0, 5.4 mg L^{-1} ozone concentration) or combined molecular radicalary attack. Experimental conditions: Q_G = 4 L min^{-1}; M_{CAT} = 3.3 g L^{-1}; T = 18.0 °C; P = 1 atm; V_{reac} = 1.5 L; (*Agitation*) = 60 rpm.

In Figure 7c, an overlap of both radical and molecular pathways can be observed, which is consistent with the kinetic parameters obtained from the Ad/Ox model, where an equilibrium situation was observed between oxidation in the liquid and on the surface of the solid through adsorption. The results obtained in the analyses carried out allow us to propose the mechanism of aniline degradation shown in Figure 8.

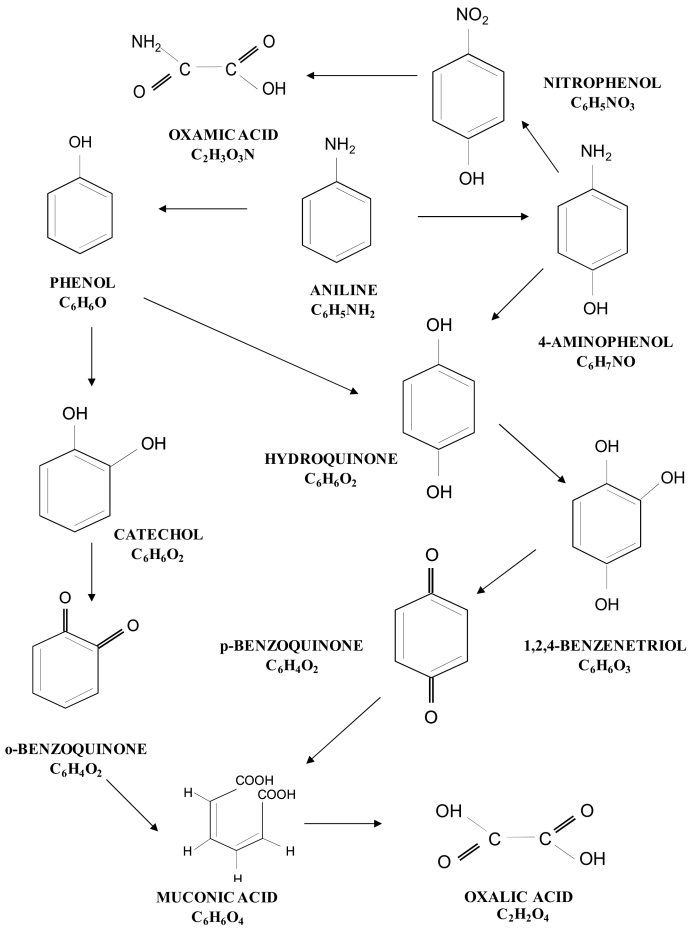

Figure 8. Oxidation pathway proposed for aniline oxidation via catalytic ozonation with TiO_2/GAC composites.

4. Conclusions

A three-phase mathematical model reaction (Ad/Ox) was proposed that describes the stages of G–L transfer, adsorption, and oxidation in the liquid and on the surface of the catalyst, in order to study catalytic ozonation using TiO_2/GAC composites. The model was verified using experimental aniline ozonation results. Despite the wide variety of conditions studied, the model provided a good fit to the experimental data, obtaining a weighted standard deviation lower than 0.05 in all cases. The model has been applied to evaluate the effect of the main operational variables on the G-L mass transfer. The analysis resulted in $K_L a$ values of 0.18 min^{-1} at neutral pH, with no significance of other process conditions and no effect on the overall process rate (chemical reaction control).

Catalytic oxidation using commercial activated carbons, such as Norit® GAC 1240 Plus, was proved to occur through a Langmuir–Hinshelwood mechanism with preferential oxidation in the liquid phase. With the TiO_2/GAC composite, the estimated oxidation constants—in the liquid and in the solid—suggest a modified Eley–Rideal type mechanism, obtaining 80.2% mineralization in the most favourable conditions. Estimation of the oxidation constants allowed us to deduce that ozone acts mainly in the liquid at acidic pH, whereas under basic pH values, oxidation happens either on the solid or in the liquid. The use of high doses of ozone limits the kinetics and adsorption capacity of aniline and its degradation oxidation products, with oxidation in the liquid being the principal route of degradation. On the other hand, at moderate ozone doses, a greater role of the adsorption and oxidation mechanisms of the TiO_2 deposited in the GAC was observed. An excess in the catalyst load was ineffective and led to an increase in turbidity by inducing degradation pathways that ended with oxidation products such as oxalic acid and, especially, oxamic acid. Finally, the model allowed us

to analyse the significance of the different stages involved in the catalytic ozonation. Additionally, the most favourable operating conditions for the potentiation of the TiO_2 deposited on the GAC were found (pH = 7.0, 5.4 mg L^{-1} ozone dose, and 3.3 g L^{-1} catalyst load). TiO_2 contributed to a greater capacity of the material to adsorb the pollutant and subsequent predisposition to be attacked by the ozone through the hydroxyl radicals generated on its surface. From the identification and analysis of the degradation intermediates, two possible routes—which occur simultaneously under the most favourable conditions mentioned above—were proposed. This model could be applied at an industrial level with new catalysts for the prediction of operating behaviour under different working conditions.

Supplementary Materials: The following are available online at http://www.mdpi.com/2073-4441/12/12/3448/s1, Figure S1: Utilization efficiencies of ozone in a TiO_2/GAC catalytic system at different pHs, Figure S2: Effect of the ozone dose on the control stage during catalytic ozonation of aniline with the TiO_2/GAC catalyst, Figure S3: Analysis of some by-products formed during the TiO_2/GAC ozonation of aniline in terms of TOC, Figure S4: Analysis of the main intermediates in the aniline catalytic ozonation with TiO_2/GAC in terms of TOC, excluding oxalic and oxamic acid in different cases.

Author Contributions: J.I.L. and C.F. performed the conceptualization; M.J.R. and J.I.L. carried out the design of the methodology and analyses; C.F. and N.V. contributed to the model validation; C.F. carried out the formal analysis; C.F. performed the investigation; C.F. and J.I.L. prepared the original draft; M.J.R., C.F. and N.V. reviewed and edited the manuscript; J.I.L. and M.J.R. supervised the experimentation; M.J.R., N.V., and J.I.L. acquired the funding. All authors have read and agreed to the published version of the manuscript.

Funding: The authors are grateful to the University of the Basque Country for their financial support of this study through the PPGA19/63 project and C. Ferreiro's predoctoral PIF grant (PIF16/367).

Acknowledgments: The authors are thankful for the technical and human support provided by The Singular Coupled Multispectroscopy Laboratory (Raman-LASPEA) and Central Analysis Service (Araba Unit), part of the General Research Services (SGIker) of the UPV/EHU, and Cabot Corporation for supplying the sample of activated carbon used in this work.

Conflicts of Interest: The authors declare no conflict of interest.

Nomenclature

σ	Weighted standard deviation
$C^*_{O_3,L}$	Concentration of ozone in the equilibrium with the ozone adsorbed on the activated carbon, mg L^{-1}
$C^*_{O_3,S}$	Concentration of ozone on the catalyst in equilibrium with the liquid ozone concentration, mg L^{-1}
C^*_p	Calculate pollutant concentration in the liquid in terms of total organic carbon, mg L^{-1}
C_N	Concentration degradation products, mg L^{-1}
$C_{O_3,in}$	Concentrations of ozone in the gas phase at the inlet, mg L^{-1}
$C_{O_3,L}$	Ozone concentration in liquid, mg L^{-1}
$C_{O_3,out}$	Concentration of ozone in the gas phase at the outlet, mg L^{-1}
C_{OH^-}	Concentration of hydroxyl ions, mol L^{-1}
C_p	Pollutant concentration in the liquid in terms of total organic carbon, mg L^{-1}
He	Henry's constant, bar L mg^{-1}
k_{ads}	Kinetic constant of aniline adsorption, g mg^{-1} min^{-1}
$k_{c,L}$	Elemental kinetic constant for the ozonation in the liquid, L mg^{-1} min^{-1}
$k_{c,S}$	Elemental kinetic constant for the ozonation in the solid, L mg^{-1} min^{-1}
K_F	Freundlich constant, (mg g^{-1}) (L mg^{-1})$^{1/nF}$
K_Ga	Overall mass transfer coefficient of ozone gas to water, min^{-1}
K_La	Volumetric ozone mass transfer coefficient, min^{-1}
k_{oxL}	Apparent first-order kinetic constant in the liquid in terms of TOC, min^{-1}
k_{oxS}	Apparent first-order kinetic constant over the catalyst in terms of TOC, min^{-1}
m	Slope of the equilibrium line between the liquid and solid phase
M_{CAT}	Concentration of catalyst, g L^{-1}
n	Heterogeneity factor, dimensionless
N	Number of experimental values
$N^{II}{}_{O3}$	Ozone consumption in the solid, mg L^{-1} min^{-1}
$N^{I}{}_{O3}$	Ozone consumption in the liquid, mg L^{-1} min^{-1}

N_{O_3}	Whole ozone consumption, mg L^{-1} min^{-1}
$P^*_{O_3}$	Partial pressure of the ozone in equilibrium with the adsorbed ozone on the solid, bar
P_{O_3}	Partial pressure of ozone in the gas phase, bar
Q_G	Ozone gas flow, L min^{-1}
$r^{II}{}_p$	Degradation of the pollutant on the activated carbon, mg L^{-1} min^{-1}
$r^{I}{}_p$	Degradation of the pollutant in the liquid, mg L^{-1} min^{-1}
T	Temperature, K
t	Time, min
U_{O_3}	Utilization coefficient, %
V_{reac}	Volume of dissolution, L
z^I	Amount of pollutant consumed in the liquid, mg TOC mg^{-1} O_3
z^{II}	Amount of pollutant consumed on the catalyst, mg TOC mg^{-1} O_3
Z_p	Concentration of pollutant in the solid, mg g^{-1}
$Z_{p,\infty}$	Amount of pollutant adsorbed in the solid in equilibrium, mg g^{-1}

References

1. United Nations. About the Sustainable Development Goals. Available online: https://www.un.org/sustainabledevelopment/sustainable-development-goals/ (accessed on 27 November 2020).
2. Zouboulis, A.I.; Katsoyiannis, I.A. Recent Advances in Water and Wastewater Treatment with Emphasis in Membrane Treatment Operations. *Water* **2019**, *11*, 45. [CrossRef]
3. Anotai, J.; Jevprasesphant, A.; Lin, Y.-M.; Lu, M.-C. Oxidation of aniline by titanium dioxide activated with visible light. *Sep. Purif. Technol.* **2012**, *84*, 132–137. [CrossRef]
4. Ferreiro, C.; Villota, N.; Lombraña, J.I.; Rivero, M.J. An efficient catalytic process for the treatment of genotoxic aniline wastewater using a new granular activated carbon-supported titanium dioxide composite. *J. Clean. Prod.* **2019**, *228*, 1282–1295. [CrossRef]
5. Ferreiro, C.; Villota, N.; Lombraña, J.I.; Rivero, M.J.; Zúñiga, V.; Rituerto, J.M. Analysis of a Hybrid Suspended-Supported Photocatalytic Reactor for the Treatment of Wastewater Containing Benzothiazole and Aniline. *Water* **2019**, *11*, 337. [CrossRef]
6. Jing, Z.; Cao, S.; Yu, T.; Hu, J. Degradation Characteristics of Aniline with Ozonation and Subsequent Treatment Analysis. *J. Chem.* **2015**, 905921. [CrossRef]
7. European Commission. *European Union Risk Assessment Report aniline*; Office for Official Publications of the European Communities: Luxembourg, 2004; Volume 50.
8. Tao, N.; Liu, G.; Bai, L.; Tang, L.; Guo, C. Genotoxicity and growth inhibition effects of aniline on wheat. *Chemosphere* **2017**, *169*, 467–473. [CrossRef]
9. United State Environmental Protection Agency. Contaminant Candidate List 4-CCL 4. Available online: https://www.epa.gov/ccl/contaminant-candidate-list-4-ccl-4-0 (accessed on 9 October 2020).
10. Alvárez, P.M.; Beltrán, F.J.; Masa, F.J.; Pocostales, J.P. A comparison between catalytic ozonation and activated carbon adsorption/ozone-regeneration processes for wastewater treatment. *Appl. Catal. B Environ.* **2009**, *92*, 393–400. [CrossRef]
11. Cheng, W.; Quan, X.; Li, R.; Wu, J.; Zhao, Q. Ozonation of Phenol-Containing Wastewater Using O_3/$Ca(OH)_2$ System in a Micro Bubble Gas-Liquid Reactor. *Ozone-Sci. Eng.* **2018**, *40*, 173–182. [CrossRef]
12. Rodríguez, A.; Rosal, R.; Perdigón-Melón, J.A.; Mezcua, M.; Agüera, A.; Hernando, M.D.; Letón, P.; Fernández-Alba, A.R.; García-Calvo, E. Ozone-Based Technologies in Water and Wastewater Treatment. In *Emerging Contaminants from Industrial and Municipal Waste. Removal Technologies*; Barceló, D., Petrovic, M., Eds.; Springer-Verlag: Heidelberg, Germany, 2008; Volume 5S/2, pp. 127–175. ISBN 978-3-540-79209-3.
13. Guo, Y.; Yang, L.; Wang, X. The Application and Reaction Mechanism of Catalytic Ozonation in Water Treatment. *J. Environ. Anal. Toxicol.* **2012**, *2*. [CrossRef]
14. Legube, B.; Karpel Vel Leitner, N. Catalytic ozonation: A promising advanced oxidation technology for water treatment. *Catal. Today* **1999**, *53*, 61–72. [CrossRef]
15. Delmas, H.; Creanga, C.; Julcour-Lebigue, C.; Wilhelm, A.-M. AD-OX: A sequential oxidative process for water treatment-Adsorption and batch CWAO regeneration of activated carbon. *Chem. Eng. J.* **2009**, *152*, 189–194. [CrossRef]

16. Erol, F.; Ozbelge, T.A.; Ozbelge, H.O. Modeling of catalytic ozonation process in a three-phase reactor. *J. Environ. Sci. Health A Tox. Hazard Subst. Environ. Eng.* **2009**, *44*, 295–306. [CrossRef] [PubMed]
17. Cheng, J.; Yang, Z.R.; Chen, H.Q.; Kuo, C.H.; Zappi, E.M. Modeling of organic pollutant destruction in a stirred-tank reactor by ozonation. *J. Environ. Sci. (China)* **2001**, *13*, 449–452.
18. Guelli Ulson de Souza, S.M.d.A.; de Souza, F.B.; Ulson de Souza, A.A. Application of Individual and Simultaneous Ozonation and Adsorption Processes in Batch and Fixed-Bed Reactors for Phenol Removal. *Ozone-Sci. Eng.* **2012**, *34*, 259–268. [CrossRef]
19. Ferreiro, C.; Villota, N.; de Luis, A.; Lombrana, J.I. Analysis of the effect of the operational variants in a combined adsorption-ozonation process with granular activated carbon for the treatment of phenol wastewater. *React. Chem. Eng.* **2020**, *5*, 760–778. [CrossRef]
20. Song, S.; He, Z.; Chen, J. US/O_3 combination degradation of aniline in aqueous solution. *Ultrason. Sonochem.* **2007**, *14*, 84–88. [CrossRef]
21. Faria, P.C.C.; Orfao, J.J.M.; Pereira, M.F.R. Ozonation of aniline promoted by activated carbon. *Chemosphere* **2007**, *67*, 809–815. [CrossRef]
22. Orge, C.A.; Faria, J.L.; Pereira, M.F.R. Photocatalytic ozonation of aniline with TiO_2-carbon composite materials. *J. Environ. Manag.* **2017**, *195*, 208–215. [CrossRef]
23. Rodriguez, C.; Ignacio Lombrana, J.; de Luis, A.; Sanz, J. Oxidizing efficiency analysis of an ozonation process to degrade the dye rhodamine 6G. *J. Chem. Technol. Biotechnol.* **2017**, *92*, 656–665. [CrossRef]
24. Byun, S.; Cho, S.H.; Yoon, J.; Geissen, S.U.; Vogelpohl, A.; Kim, S.M. Influence of mass transfer on the ozonation of wastewater from the glass fiber industry. *Water Sci. Technol.* **2004**, *49*, 31–36. [CrossRef]
25. Christopher, R.; Schulz, P.E.; Paul, W. Prendiville P.E. Designing High Concentration Ozone Contactors for Drinking Water Treatment Plants. *Ozone Sci. Eng.* **1993**, *15*, 245–266. [CrossRef]
26. Roth, J.; Sullivan, D. Solubility of Ozone in Water. *Ind. Eng. Chem. Fundam.* **1981**, *20*, 137–140. [CrossRef]
27. Egorova, G.V.; Voblikova, V.A.; Sabitova, L.V.; Tkachenko, I.S.; Tkachenko, S.N.; Lunin, V.V. Ozone Solubility in Water. *Moscow Univ. Chem. Bull.* **2015**, *70*, 207–210. [CrossRef]
28. Beltran, F.J. *Ozone Reaction Kinetics for Water and Wastewater Systems*; CRC Press: Boca Ratón, FL, USA, 2003; ISBN 978-0-203-50917-3.
29. Cacace, F.; Speranza, M. Protonated Ozone: Experimental Detection of O_3H^+ and Evaluation of the Proton Affinity of Ozone. *Science* **1994**, *265*, 208–209. [CrossRef] [PubMed]
30. Flores-Payán, V.; Herrera-López, E.J.; Navarro-Laboulais, J.; López-López, A. Parametric sensitivity analysis and ozone mass transfer modeling in a gas–liquid reactor for advanced water treatment. *J. Ind. Eng. Chem.* **2015**, *21*, 1270–1276. [CrossRef]
31. Ratnawati, R.; Kusumaningtyas, D.; Suseno, P.; Prasetyaningrum, A. Mass Transfer Coefficient of Ozone in a Bubble Column. *MATEC Web Conf.* **2018**, *156*, 02015. [CrossRef]
32. Berry, M.J.; Taylor, C.M.; King, W.; Chew, Y.M.J.; Wenk, J. Modelling of Ozone Mass-Transfer through Non-Porous Membranes for Water Treatment. *Water* **2017**, *9*, 452. [CrossRef]
33. VonSonntag, C.; VonGunten, U. *Chemistry of Ozone in Water and Wastewater Treatment: From Basic Principles to Applications*; Iwa Publishing: London, UK, 2012; ISBN 978-1-84339-313-9.
34. Masel, R.I. *Principles of Adsorption and Reaction on Solid Surfaces*, 1st ed.; Wiley: Oak Brook, IL, USA, 1996.
35. De Luis, A.; Lombraña, J.I. pH-Based Strategies for an Efficient Addition of H_2O_2 During Ozonation to Improve the Mineralisation of Two Contaminants with Different Degradation Resistances. *Water Air Soil Pollut.* **2018**, *229*, 372. [CrossRef]
36. Wang, B.; Zhang, H.; Wang, F.; Xiong, X.; Tian, K.; Sun, Y.; Yu, T. Application of Heterogeneous Catalytic Ozonation for Refractory Organics in Wastewater. *Catalysts* **2019**, *9*, 241. [CrossRef]
37. Zheng, X.; Yu, N.; Wang, X.; Wang, Y.; Wang, L.; Li, X.; Hu, X. Adsorption Properties of Granular Activated Carbon-Supported Titanium Dioxide Particles for Dyes and Copper Ions. *Sci. Rep.* **2018**, *8*, 6463. [CrossRef]
38. Kasprzyk-Hordern, B.; Ziółek, M.; Nawrocki, J. Catalytic ozonation and methods of enhancing molecular ozone reactions in water treatment. *Appl. Catal. B Environ.* **2003**, *46*, 639–669. [CrossRef]
39. Valdes, H.; Sanchez-Polo, M.; Rivera-Utrilla, J.; Zaror, C.A. Effect of ozone treatment on surface properties of activated carbon. *Langmuir* **2002**, *18*, 2111–2116. [CrossRef]
40. Ghuge, S.P.; Saroha, A.K. Catalytic ozonation for the treatment of synthetic and industrial effluents—Application of mesoporous materials: A review. *J. Environ. Manag.* **2018**, *211*, 83–102. [CrossRef] [PubMed]

41. Moussavi, G.; Khavanin, A.; Alizadeh, R. The investigation of catalytic ozonation and integrated catalytic ozonation/biological processes for the removal of phenol from saline wastewaters. *J. Hazard. Mater.* **2009**, *171*, 175–181. [CrossRef] [PubMed]
42. Sanchez, M.; Rivero, M.J.; Ortiz, I. Kinetics of dodecylbenzenesulphonate mineralisation by TiO_2 photocatalysis. *Appl. Catal. B Environ.* **2011**, *101*, 515–521. [CrossRef]
43. MiarAlipour, S.; Friedmann, D.; Scott, J.; Amal, R. TiO_2/porous adsorbents: Recent advances and novel applications. *J. Hazard. Mater.* **2018**, *341*, 404–423. [CrossRef] [PubMed]
44. Beltran, F.J.; Rivas, F.J.; Montero-de-Espinosa, R. A TiO_2/Al_2O_3 catalyst to improve the ozonation of oxalic acid in water. *Appl. Catal. B-Environ.* **2004**, *47*, 101–109. [CrossRef]
45. Vega, E.; Valdes, H. New evidence of the effect of the chemical structure of activated carbon on the activity to promote radical generation in an advanced oxidation process using hydrogen peroxide. *Microporous Mesoporous Mat.* **2018**, *259*, 1–8. [CrossRef]
46. Orge, C.A.; Sousa, J.P.S.; Gonçalves, F.; Freire, C.; Órfão, J.J.M.; Pereira, M.F.R. Development of Novel Mesoporous Carbon Materials for the Catalytic Ozonation of Organic Pollutants. *Catal. Lett.* **2009**, *132*, 1–9. [CrossRef]
47. Turhan, K.; Uzman, S. The degradation products of aniline in the solutions with ozone and kinetic investigations. *Ann. Chim.* **2007**, *97*, 1129–1138. [CrossRef]
48. Shahamat, Y.D.; Farzadkia, M.; Nasseri, S.; Mahvi, A.H.; Gholami, M.; Esrafili, A. Magnetic heterogeneous catalytic ozonation: A new removal method for phenol in industrial wastewater. *J. Environ. Health Sci. Eng.* **2014**, *12*, 50. [CrossRef] [PubMed]
49. Boczkaj, G.; Fernandes, A. Wastewater treatment by means of advanced oxidation processes at basic pH conditions: A review. *Chem. Eng. J.* **2017**, *320*, 608–633. [CrossRef]
50. Roshani, B.; McMaster, I.; Rezaei, E.; Soltan, J. Catalytic ozonation of benzotriazole over alumina supported transition metal oxide catalysts in water. *Sep. Purif. Technol.* **2014**, *135*, 158–164. [CrossRef]
51. Nawrocki, J.; Kasprzyk-Hordern, B. The efficiency and mechanisms of catalytic ozonation. *Appl. Catalysis B Environ.* **2010**, *99*, 27–42. [CrossRef]
52. Tamura, H.; Mita, K.; Tanaka, A.; Ito, M. Mechanism of Hydroxylation of Metal Oxide Surfaces. *J. Colloid Interface Sci.* **2001**, *243*, 202–207. [CrossRef]
53. Valdés, H.; Sánchez-Polo, M.; Zaror, C.A. Role of oxygen-containing functional surface groups of activated carbons on the elimination of 2-hydroxybenzothiazole from waters in A hybrid heterogeneous ozonation system. *J. Adv. Oxid. Technol.* **2017**, *20*. [CrossRef]
54. Orha, C.; Pode, R.; Manea, F.; Lazau, C.; Bandas, C. Titanium dioxide-modified activated carbon for advanced drinking water treatment. *Process Saf. Environ. Protect.* **2017**, *108*, 26–33. [CrossRef]
55. Beltrán, F.J.; Rivas, J.; Álvarez, P.; Montero-de-Espinosa, R. Kinetics of Heterogeneous Catalytic Ozone Decomposition in Water on an Activated Carbon. *Ozone Sci. Eng.* **2002**, *24*, 227–237. [CrossRef]
56. Leyva, E.; Moctezuma, E.; Noriega, S. Photocatalytic degradation of omeprazole. Intermediates and total reaction mechanism. *J. Chem. Technol. Biotechnol.* **2017**, *92*, 1511–1520. [CrossRef]
57. Bulanin, K.M.; Lavalley, J.C.; Tsyganenko, A.A. Infrared Study of Ozone Adsorption on TiO_2 (Anatase). *J. Phys. Chem.* **1995**, *99*, 10294–10298. [CrossRef]
58. Bodzek, M.; Rajca, M. Photocatalysis in the treatment and disinfection of water. Part I. Theoretical backgrounds. *Ecol. Chem. Eng. S* **2012**, *19*, 489–512. [CrossRef]
59. Orge, C.A.; Faria, J.L.; Pereira, M.F.R. Removal of oxalic acid, oxamic acid and aniline by a combined photolysis and ozonation process. *Environ. Technol.* **2015**, *36*, 1075–1083. [CrossRef] [PubMed]
60. Zazo, J.A.; Casas, J.A.; Mohedano, A.F.; Gilarranz, M.A.; Rodríguez, J.J. Chemical Pathway and Kinetics of Phenol Oxidation by Fenton's Reagent. *Environ. Sci. Technol.* **2005**, *39*, 9295–9302. [CrossRef] [PubMed]
61. Faria, P.C.C.; Órfão, J.J.M.; Pereira, M.F.R. Activated carbon catalytic ozonation of oxamic and oxalic acids. *Appl. Catal. B Environ.* **2008**, *79*, 237–243. [CrossRef]
62. Villota, N.; Lombraña, J.I.; Cruz-Alcalde, A.; Marcé, M.; Esplugas, S. Kinetic study of colored species formation during paracetamol removal from water in a semicontinuous ozonation contactor. *Sci. Total Environ.* **2019**, *649*, 1434–1442. [CrossRef] [PubMed]
63. Mijangos, F.; Varona, F.; Villota, N. Changes in Solution Color During Phenol Oxidation by Fenton Reagent. *Environ. Sci. Technol.* **2006**, *40*, 5538–5543. [CrossRef] [PubMed]

64. Villota, N.; Lomas, J.M.; Camarero, L.M. Study of the paracetamol degradation pathway that generates color and turbidity in oxidized wastewaters by photo-Fenton technology. *J. Photochem. Photobiol. A Chem.* **2016**, *329*, 113–119. [CrossRef]
65. Rasalingam, S.; Kibombo, H.S.; Wu, C.-M.; Peng, R.; Baltrusaitis, J.; Koodali, R.T. Competitive role of structural properties of titania–silica mixed oxides and a mechanistic study of the photocatalytic degradation of phenol. *Appl. Catal. B Environ.* **2014**, *148–149*, 394–405. [CrossRef]
66. Anpo, M.; Kamat, P.V. (Eds.) *Environmentally Benign Photocatalysts: Applications of Titanium Oxide-based Materials*; Nanostructure Science and Technology; Springer: New York, NY, USA, 2010; ISBN 978-0-387-48441-9.
67. Brillas, E.; Bastida, R.M.; Llosa, E.; Casado, J. Electrochemical Destruction of Aniline and 4-Chloroaniline for Wastewater Treatment Using a Carbon-PTFE O_2—Fed Cathode. *J. Electrochem. Soc.* **1995**, *142*, 1733. [CrossRef]
68. Tolosana-Moranchel, A.; Montejano, A.; Casas, J.A.; Bahamonde, A. Elucidation of the photocatalytic-mechanism of phenolic compounds. *J. Environ. Chem. Eng.* **2018**, *6*, 5712–5719. [CrossRef]
69. Sánchez, L.; Peral, J.; Domènech, X. Photocatalyzed destruction of aniline in UV-illuminated aqueous TiO_2 suspensions. *Electrochim. Acta* **1997**, *42*, 1877–1882. [CrossRef]
70. Comninellis, C.; Pulgarin, C. Anodic oxidation of phenol for waste water treatment. *J. Appl. Electrochem.* **1991**, *21*, 703–708. [CrossRef]